NeuroImage 282 (2023) 120387

Contents lists available at ScienceDirect

NeuroImage

journal homepage: www.elsevier.com/locate/ynimg

High resolution 0.5mm isotropic T_1-weighted and diffusion tensor templates of the brain of non-demented older adults in a common space for the MIITRA atlas

Yingjuan Wu [a,#], Abdur Raquib Ridwan [a,#], Mohammad Rakeen Niaz [a], Alzheimer's Disease Neuroimaging Initiative[$], David A. Bennett [b], Konstantinos Arfanakis [a,b,*]

[a] Department of Biomedical Engineering, Illinois Institute of Technology, Chicago, IL, United States
[b] Rush Alzheimer's Disease Center, Rush University Medical Center, Chicago, IL, United States

ARTICLE INFO

Keywords:
Brain
Template
Multimodal
High resolution
T_1-weighted
Diffusion tensor imaging
Aging

ABSTRACT

High quality, high resolution T_1-weighted (T_1w) and diffusion tensor imaging (DTI) brain templates located in a common space can enhance the sensitivity and precision of template-based neuroimaging studies. However, such multimodal templates have not been constructed for the older adult brain. The purpose of this work which is part of the MIITRA atlas project was twofold: (A) to develop 0.5 mm isotropic resolution T_1w and DTI templates that are representative of the brain of non-demented older adults and are located in the same space, using advanced multimodal template construction techniques and principles of super resolution on data from a large, diverse, community cohort of 400 non-demented older adults, and (B) to systematically compare the new templates to other standardized templates. It was demonstrated that the new MIITRA-0.5mm T_1w and DTI templates are well-matched in space, exhibit good definition of brain structures, including fine structures, exhibit higher image sharpness than other standardized templates, and are free of artifacts. The MIITRA-0.5mm T_1w and DTI templates allowed higher intra-modality inter-subject spatial normalization precision as well as higher inter-modality intra-subject spatial matching of older adult T_1w and DTI data compared to other available templates. Consequently, MIITRA-0.5mm templates allowed detection of smaller inter-group differences for older adult data compared to other templates. The MIITRA-0.5mm templates were also shown to be most representative of the brain of non-demented older adults compared to other templates with submillimeter resolution. The new templates constructed in this work constitute two of the final products of the MIITRA atlas project and are anticipated to have important implications for the sensitivity and precision of studies on older adults.

1. Introduction

High quality T_1-weighted (T_1w) and diffusion tensor imaging (DTI) brain templates are indispensable tools in neuroimaging (Evans et al., 2012; Fonov et al., 2009; Joshi et al., 2004; Mazziotta et al., 2001; Zhang and Arfanakis, 2018). Due to the advantages of integrating structural and diffusion MRI information in voxel-wise multivariate statistical analyses, T_1w and DTI templates that are located in a common space are highly desirable (Calhoun and Sui, 2016; Avants et al., 2008a, 2010a; Kim et al., 2015; Kochunov et al., 2007; Sasamoto et al., 2014; Sydykova et al., 2007; Toga et al., 2006). In addition, recent developments in image acquisition, reconstruction and enhancement (Jia et al., 2016; Wiggins et al., 2006; Zhang et al., 2009; Sánchez and Vilaplana, 2018; Zeng et al., 2018), and in neuroimaging software (Manjón et al., 2020; Park et al., 2014), have made it possible to study the brain at submillimeter resolution (Bookheimer et al., 2019; Van

* Corresponding author: Konstantinos Arfanakis, 3440 S Dearborn St, M-100, Illinois Institute of Technology, Chicago, Illinois 60616, United States.
E-mail address: arfanakis@iit.edu (K. Arfanakis).
[#] Contributed equally.
[$] A portion of the data used in preparation of this article were obtained from the Alzheimer's Disease Neuroimaging Initiative (ADNI) database (adni.loni.usc.edu). As such, the investigators within the ADNI contributed to the design and implementation of ADNI and/or provided data but did not participate in analysis or writing of this report. A complete listing of ADNI investigators can be found at: http://adni.loni.usc.edu/wp-content/uploads/how-to-apply/ADNI-Acknowledgement-List.pdf.

https://doi.org/10.1016/j.neuroimage.2023.120387
Received 10 August 2023; Accepted 22 September 2023
Available online 1 October 2023

Leemput et al., 2008; Yushkevich et al., 2015), increasing the demand for templates with high spatial resolution (Yushkevich et al., 2009; Zhao et al., 2016). Furthermore, due to well-known age-related brain changes (Blatter et al., 1995; Cox et al., 2016; Ge et al., 2002; Lemaître et al., 2005; Raz et al., 2005; Sullivan et al., 2006, 2010; Westlye et al., 2010), it is essential for studies on older adults to use T_1w and DTI brain templates that are representative of the older adult brain in order to avoid registration errors or biases (Fonov et al., 2011; Good et al., 2001; Ridwan et al., 2021a; Senjem et al., 2005; Yoon et al., 2009). However, multimodal T_1w and DTI templates that are located in the same space and have submillimeter resolution are not available for the older adult brain.

Multimodal T_1w and DTI templates can be constructed using three approaches. One approach is based on single-channel registration and can either optimize spatial matching of templates across modalities as well as template quality for only one modality at the cost of low template quality for the other modality (Gupta et al., 2016; Mori et al., 2008; Rohlfing et al., 2010), or can optimize template quality for both modalities separately at the cost of reduced template matching across modalities (Hsu et al., 2015). To address these limitations, a second approach uses multichannel registration aiming at both high template quality and excellent template matching across modalities (Arthofer et al., 2021; Avants et al., 2008a; Irfanoglu et al., 2016; Lange et al., 2020; Li and Verma, 2011; Park et al., 2003). However, due to the drastically different contrast between T_1w and DTI images, the requirement in multichannel registration for simultaneous optimization of inter-subject spatial matching in both T_1w and DTI data may lead to less precise spatial matching of the features of interest in each modality compared to considering each modality separately, thereby compromising the quality of both templates (Wu et al., 2022). For those reasons, a third, iterative approach was introduced recently which uses single modality registration in data from multiple individuals to maximize the quality of one template and applies the resulting transformations to data from both modalities, then uses single modality registration to maximize the quality of the other template and applies the resulting transformations to data from both modalities, and repeats these steps iteratively (Wu et al., 2022). Multiple iterations enhance both the quality and spatial matching of the two templates. This approach was successful in generating multimodal T_1w and DTI templates that exhibited higher image quality and excellent spatial matching and allowed overall higher inter-subject and inter-modality spatial normalization precision for external data compared to templates generated using state-of-the-art multichannel registration. Although these were templates of the older adult brain they were constructed with 1 mm isotropic resolution.

A conventional approach for building templates with submillimeter resolution is to use data that also have submillimeter resolution. However, one major limitation of this approach is the complexity of acquiring high resolution MRI data from a large number of older adults due to long acquisition times, motion artifacts, and/or low signal to noise ratio. Niaz et al. (2022) addressed this limitation by constructing a high resolution population-based T_1w brain template from lower resolution images on individual subjects using the concept of multiple image super resolution and considering every co-registered image as a different realization of the template brain. The resulting high resolution T_1w template improved visualization of fine structural details, allowed higher spatial normalization precision for external data and enabled detection of smaller inter-group morphometric differences compared to the template generated using conventional template building methods (Niaz et al., 2022). However, this approach has so far only been tested on single channel T_1w images.

The purpose of the present work was twofold: (A) to develop multimodal T_1w and DTI templates that are representative of the brain of non-demented older adults, located in the same space, and have submillimeter resolution, using advanced multimodal template construction techniques and principles of super resolution, and (B) to systematically compare the new templates to other standardized templates. First, high quality T_1w and DTI data were collected on a large, diverse, community cohort of 400 non-demented older adults. An initial template was constructed by pairwise affine registration to minimize biases towards any participant's images or any existing templates. Next, T_1w and DTI data were spatially normalized using the iterative multimodal template building approach introduced by Wu et al. (2022) that aims at maximizing the quality and spatial matching of the two templates. The resulting spatial transformations were used to forward-map signals to exact physical locations in template space and using principles of super resolution the final T_1w and DTI templates were generated. Finally, the new templates were compared to those of other standardized templates in terms of image quality and performance when used as reference for alignment of older adult data. The new templates constitute two of the final products of the project to develop a comprehensive older adult brain atlas named Multichannel Illinois Institute of Technology & Rush university Aging (MIITRA) atlas, and are available for download at www.nitrc.org/projects/miitra.

2. Methods

2.1. Data

Two older adult brain MRI datasets were used in this work. Dataset 1 was used in the construction of the new high resolution multimodal T_1w and DTI templates. It consisted of structural T_1w and diffusion-weighted data collected on 400 non-demented older adults (50% male; 64.9–98.9 years age range; mean±sd age=79.9±7.1 years; 79.5% had no cognitive impairment and 20.5% had mild cognitive impairment; 54% white and 43% black; 7% Latino) participating in the Rush Memory and Aging Project (Bennett et al., 2018), Minority Aging Research Study (Barnes et al., 2012), Religious Orders Study (Bennett et al., 2018), and Clinical Core and Latino Core of the Rush Alzheimer's Disease Research Center (Marquez et al., 2020). All studies were approved by the institutional committee for the protection of human subjects and all participants provided written informed consent. All data were acquired on a 3T Siemens Trio (188 persons) and a 3T Philips Achieva MRI scanner (212 persons). T_1w images were acquired using a 3D magnetization prepared rapid acquisition gradient echo (MPRAGE) sequence with the following parameters: 3T Siemens Trio: TR = 2300 ms, TE = 2.98 ms, TI = 900 ms, flip-angle = 9°, field of view (FOV) = 256 × 256 mm^2, 176 sagittal slices, acquired voxel size=1 × 1 × 1 mm^3, and an acceleration factor of 2; 3T Philips Achieva: TR = 8 ms, TE = 3.7 ms, TI = 955 ms, flip-angle = 8°, FOV = 240 × 228 mm^2, 181 sagittal slices, acquired voxel size=1 × 1 × 1 mm^3, and an acceleration factor of 2. The diffusion data were obtained using a spin-echo echo-planar diffusion-weighted imaging sequence with the following parameters: 3T Siemens Trio: TR = 8100 ms, TE = 85 ms, FOV = 224 × 224 mm^2, 65 axial slices, acquired voxel size = 2 × 2 × 2 mm^3, b = 1000s/mm^2 for 40 diffusion gradient directions, and 6 volumes with b = 0 s/mm^2; 3T Philips Achieva: TR = 10, 701 ms, TE = 55 ms, and all other parameters were the same.

Dataset 2 was used in the evaluation of the performance of the different templates considered in this work. It consisted of T_1w and diffusion-weighted data from 202 non-demented older adults (50% male; 65–93.2 years age range; mean±sd age = 78.3±6.0 years; 122 had no cognitive impairment and 80 had mild cognitive impairment) participating in the Alzheimer's Disease Neuroimaging Initiative 3 (ADNI3) (http://adni.loni.usc.edu). ADNI was established as a public-private partnership under the leadership of Principal Investigator Michael W. Weiner, MD in 2003 to investigate whether serial MRI, positron emission tomography (PET), other biological markers, and clinical and neuropsychological assessment can be combined to measure the progression of mild cognitive impairment and early Alzheimer's disease. All data in Dataset 2 were collected on 3T Siemens (146 persons) and 3T Philips (56 persons) MRI scanners. T_1w images were obtained using 3D MPRAGE sequences with the following parameters: 3T Siemens Prisma (92 persons), Verio (23 persons), Trio (22 persons) and

Skyra (9 persons): TR=2300 ms, TE=2.98 ms, TI=900 ms, flip-angle=9°, FOV=256 × 240 mm^2, 208/176/176/176 sagittal slices respectively, voxel size=1 × 1 × 1 mm^3, and an acceleration factor of 2; 3T Philips Achieva (40 persons) and Ingenia (16 persons): TR=6.5 ms, TE=2.9 ms, TI=900 ms, flip-angle=9°, FOV=256 × 256 mm^2, 211 sagittal slices, voxel size=1 × 1 × 1 mm^3, and an acceleration factor of 2. The diffusion data were acquired using spin-echo echo-planar diffusion-weighted sequences with the following parameters: Siemens Prisma (92 persons) and Skyra (9 persons): TR=7200 and 9600 ms respectively, TE=56 and 82 ms respectively, FOV=232 × 232 mm^2, 80 axial slices, voxel size=2 × 2 × 2 mm^3, b = 1000s/mm^2 for 48 diffusion gradient directions, and 7 volumes with b = 0 s/mm^2; Siemens Verio (23 persons) and Trio (22 persons): TR = 12,500 and 12,400 ms respectively, TE = 95 ms, FOV = 232 × 232 mm^2, 80 axial slices, voxel size=2 × 2 × 2 mm^3, b = 1000s/mm^2 for 30 diffusion gradient directions and one volume with b = 0 s/mm^2; Philips Achieva (40 persons) and Ingenia (16 persons): TR=9916 and 10,861 ms respectively, TE=86 and 100 ms respectively, FOV=256 × 256 mm^2, 80 axial slices, voxel size=2 × 2 × 2 mm^3, b = 1000s/mm^2 for 32 diffusion directions, and one volume with b = 0 s/mm^2.

2.2. Image preprocessing

T_1w images in both Datasets 1 and 2 were skull-stripped using the automated brain extraction tool HD-BET (Isensee et al., 2019). The brain images were then segmented using CAT12 (Farokhian et al., 2017) and the tissue masks were used as priors for N4 bias field inhomogeneity correction of the T_1w images (Tustison et al., 2010). The intensities of the resulting images were normalized to the range [0,100] through piecewise linear histogram matching (Nyúl et al., 2000; Shah et al., 2011) as implemented in the python package by Reinhold et al., 2019. In addition, the gray matter in Dataset 2 was segmented into the Desikan-Killiany regions using FreeSurfer (Fischl, 2012; McCarthy et al., 2015). Diffusion-weighted images in both Datasets 1 and 2 were corrected for motion, eddy-currents and EPI distortions, the B-matrix was reoriented, and diffusion tensors were computed in each brain voxel using TORTOISE and the RESTORE nonlinear fitting option (Irfanoglu et al., 2017; Pierpaoli et al., 2010; Rohde et al., 2004; Chang et al., 2005, 2012). Next, for every participant in Dataset 1, the T_1w and DTI data were up-sampled to 0.5 mm isotropic resolution through voxel splitting (no interpolation), the b = 0 s/mm^2 images were affinely registered to the T_1w images using ANTs with mutual information as the cost function (Avants et al., 2009, 2011), and the resulting transformation was applied to the diffusion tensors. The spatial matching between the T_1w and DTI data was verified by visual inspection. The co-registered T_1w and DTI data of Dataset 1 were used for template construction.

2.3. Template construction

The template construction process can be divided into 7 steps (Fig. 1). Briefly, in step 1, a minimum transformation initial T_1w template was generated to minimize biases towards any participant's images or any existing templates (Ridwan et al., 2021b; Seghers et al., 2004). Steps 2 to 5 included the iterative multimodal template building approach introduced by Wu et al. (2022). In step 6, the resulting transformations were combined and were used to forward-map signals from native space to exact physical locations in template space, and super resolution principles were applied as in Niaz et al. (2022). Lastly, in step 7, a patch-based sparse representation data fusion technique was employed to combine signals across participants into the final templates while reducing the effects of any residual misregistration (Ridwan et al., 2021b; Shi et al., 2014). The template construction process is described in more detail below.

In step 1, an unbiased initial T_1w template was generated in a reference-free manner (Ridwan et al., 2021b; Seghers et al., 2004). T_1w images (after the preprocessing of Section 2.2) were first center-aligned using linear translations, and then spatially normalized by computing pairwise affine transformations (400 × 399=159,600 registrations) using ANTs (Avants et al., 2009, 2011). Mutual information was used as the cost function for affine registration. For each participant, the mean affine transform to all other participants was computed and combined with the center alignment translation. The combined transform was then applied to the preprocessed T_1w images to bring them to a common space with a single interpolation. A T_1w template was generated from the spatially normalized T_1w images using simple averaging, and was used as an initial template in the following step. (Note that step 1 was not conducted for DTI data because of the design of the iterative multimodal template building approach introduced by Wu et al. (2022); see next steps)

In step 2, T_1w-based inter-subject spatial normalization was performed on the T_1w images from step 1 according to the approach described in Ridwan et al. (2021a) and Wu et al. (2022), which uses the symmetric group-wise normalization (SyGN) method (Avants et al., 2010b). The nonlinear registration step was initiated by setting the regularization kernel to Gauss[3,1] and was repeated for multiple iterations until the Pearson cross-correlation similarity index across T_1w templates from successive iterations was higher than 0.9995 (Ridwan et al., 2021a). The regularization kernel was then changed to Gauss[3,0] (to allow higher amounts of warping) and nonlinear registration was repeated for multiple iterations until the Pearson cross-correlation similarity index reached again a value higher than 0.9995. The transformations resulting from step 2 were combined with transformations from previous steps, and the resulting transforms were applied to the preprocessed T_1w and DTI data from Section 2.2 to bring them to a common space with a single interpolation. In this and other steps that included transformation of DTI data, diffusion tensors were reoriented based on the local rotation information of the corresponding deformation field.

In step 3, DTI-based inter-subject spatial normalization was performed on the DTI data from step 2 following the procedure described in Wu et al. (2022), which uses the non-linear registration component of DR-TAMAS (dtireg-create-template.sh) (Irfanoglu et al., 2016). The transformations resulting from step 3 were combined with those from previous steps, and the resulting transforms were applied to the preprocessed T_1w and DTI data from Section 2.2 to bring them to a common space with a single interpolation. Steps 4 and 5 included a second iteration of steps 2 and 3, respectively.

In step 6, images were forward-mapped from native space to

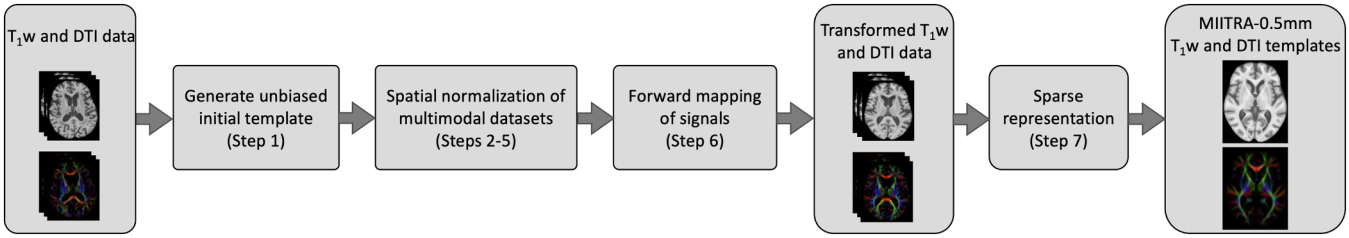

Fig. 1. Schematic representation of the approach used for the construction of the MIITRA-0.5mm T_1w and DTI templates of the older adult brain.

template space following the strategy described in Niaz et al. (2020, 2022). More specifically, for each participant, the transformation from previous steps was combined with an additional linear transformation for ac-pc alignment computed by the acpcdetect program of the Automatic Registration Toolbox (ATRA) (Ardekani and Bachman, 2009), and the single transformation was inverted and used to map the signals from native space (after the preprocessing of Section 2.2) to exact physical locations in template space with sub-voxel accuracy. In voxels where more than one signals from the same participant were mapped to, the final signal for that participant was calculated by applying Gaussian weighted averaging. Voxels without any signal from a participant were filled using conventional backward transformation (instead of forward mapping) of the participant's images using trilinear interpolation.

In step 7, a patch-based sparse-representation data fusion technique described in Shi et al. (2014) was applied on the transformed T_1w and DTI images from all participants to construct the final templates (Ridwan et al., 2021b). This approach was preferred over simple averaging to reduce the impact of any residual spatial mismatch across participants on the final templates. Finally, skull and other head structures were added to the final T_1w template using the strategy by Rohlfing et al. (Rohlfing et al., 2012; Ridwan et al., 2021a; Niaz et al., 2022). However, the brain-only templates were considered in the following evaluation. The final templates are referred to as MIITRA-0.5mm T_1w and DTI templates in the rest of this work (Fig. 2) and are available for download at www.nitrc.org/projects/miitra.

2.4. Comparison of MIITRA-0.5mm T_1w and DTI templates to other standardized templates

The MIITRA-0.5mm T_1w template was compared to other standardized T_1w templates with ≤1 mm isotropic voxels, few of which were constructed using at least some data on older adults: three templates with 0.5 mm isotropic voxels, namely (a) MCALT v1.4 (Schwarz et al., 2017), (b) ICBM2009b Asym (Fonov et al., 2009, 2011), and (c) Colin27 (Aubert-Broche et al., 2006; Holmes et al., 1998), (d) HCP-1200 with 0.7 mm isotropic voxels (Glasser et al., 2013), and two templates with 1 mm isotropic voxels, namely (e) MIITRA-1mm-2021 (Ridwan et al., 2021a), and (f) Oxford-MM-0 (Arthofer et al., 2021) (Table 1). Importantly, MIITRA-1mm-2021 was previously compared to approximately 20 other T_1w templates (Ridwan et al., 2021a), and therefore by comparing to MIITRA-1mm-2021 it is possible to indirectly compare to all those other templates. The MIITRA-0.5mm DTI template was also compared to other standardized DTI templates with different voxel-sizes: two templates with 1 mm isotropic voxels, namely (a) Oxford-MM-0 (Arthofer et al., 2021) and (b) ICBM81 (Mori et al., 2008), and (c) IXI aging v2.0 (Zhang et al., 2010) with $1.75 \times 1.75 \times 2.25$ mm^3 voxels (Table 1). No other DTI template with sub-millimeter resolution is currently available and therefore the comparison was limited to templates that included at least some data on middle-aged or older adult individuals. The MIITRA-0.5mm T_1w and DTI templates were compared to the above templates in terms of image quality, inter-subject spatial normalization precision for older adult data, ability to detect small inter-group differences, and representativeness of the older adult brain. The MIITRA-0.5mm templates were also compared to the following pairs of T_1w and DTI templates in terms of inter-modality spatial normalization precision for older adult data: (a) Oxford-MM-0 T_1w and DTI templates (Arthofer et al., 2021) and (b) MNI152 T_1w (Grabner et al., 2006) and ICBM81 DTI templates (Mori et al., 2008). More details on how the evaluation was conducted are provided below.

2.4.1. Evaluation of templates in terms of image quality, inter-subject and inter-modality spatial normalization precision of older adult data

The image quality of T_1w and DTI templates was evaluated by visual inspection as well as quantitatively. Image sharpness was assessed by means of the normalized power spectra along the anterior-posterior (AP), left-right (LR) and superior-inferior (SI) axes separately (Niaz et al., 2022).

The precision of inter-subject and inter-modality spatial normalization of older adult data from Dataset 2 when using the different templates as reference was compared across templates. More specifically, T_1w and DTI data from Dataset 2 were registered to each T_1w template using ANTs and to each DTI template using DR-TAMAS. All registrations used symmetric normalization (SyN) diffeomorphic transformation (Avants et al., 2008b), one of the top-performing transformation models (Klein et al., 2009). The precision of intra-modality inter-subject spatial normalization of T_1w images from Dataset 2 was first assessed by means of the pairwise normalized cross-correlation (PNCC) of spatially normalized T_1w images (Ferreira et al., 2014; Wang et al., 2004):

$$PNCC_{ij} = \frac{1}{N} \times \frac{\sum_{x=1}^{N} (S_i(x) - \mu_i) \times (S_j(x) - \mu_j)}{\sigma_i \times \sigma_j}, \quad (1)$$

where $S_i(x)$ and $S_j(x)$ are the signals of participants i and j at voxel x, μ_i, σ_i and μ_j, σ_j are the mean and standard deviation of the intensities of all the voxels of subjects i and j, and N is the total number of voxels. The average PNCC over all pairs of spatially normalized T_1w images of Dataset 2 ($202 \times 201/2 = 20{,}301$ pairs) was compared across T_1w templates using one-way ANOVA followed by the Tukey-Kramer post-hoc test. Differences with $p<0.05$ were considered significant. In addition, the transformations of T_1w images of Dataset 2 to each T_1w template were applied to the corresponding white matter masks of Dataset 2 and the pairwise Jaccard index (JI) of white matter masks in the space of each T_1w template was calculated as follows:

$$JI_{ij} = \frac{M_i \cap M_j}{M_i \cup M_j}, \quad (2)$$

where $M_i \cap M_j$ and $M_i \cup M_j$ are the intersection and union of the white matter masks of participants i and j. The average JI over all pairs of transformed white matter masks ($202 \times 201/2 = 20{,}301$ pairs) was compared across T_1w templates using one-way ANOVA followed by the Tukey-Kramer post-hoc test. Differences were considered significant at $p<0.05$. The same approach was used to assess the pairwise JI of gray matter masks and the pairwise JI of ventricle masks for each T_1w template.

The precision of intra-modality inter-subject spatial normalization of DTI data from Dataset 2 was first assessed by means of the pairwise Euclidean distance of tensors (DTED) (Alexander and Gee, 2000; Zhang et al., 2011; Wang et al., 2022):

$$DTED = \sqrt{trace\left((\boldsymbol{D_i} - \boldsymbol{D_j})^2\right)}, \quad (3)$$

where $\boldsymbol{D_i}$ and $\boldsymbol{D_j}$ are diffusion tensors of participants i and j in the same voxel. The average DTED over all pairs of spatially normalized DTI data of Dataset 2 ($202 \times 201/2 = 20{,}301$ pairs) was calculated in each voxel, and cumulative distributions of the average DTED in white matter were compared across DTI templates using the one-sided two-sample Kolmogorov-Smirnov (KS) test. Differences were considered significant at $p<0.05$. Second, the coherence of primary eigenvectors (COH) (Zhang et al., 2011; Irfanoglu et al., 2016) from spatially normalized DTI data of Dataset 2 was estimated using:

$$COH = 1 - \sqrt{\frac{\beta_2 + \beta_3}{2\beta_1}}, \quad (4)$$

where β_1, β_2, β_3 are the primary, secondary, and tertiary eigenvalues of the mean dyadic tensor given by:

$$\bar{\mathscr{E}} = \frac{1}{N} \sum_{i=1}^{N} e_1^i e_1^{i^T}, \quad (5)$$

where e_1^i is the primary eigenvector of participant i, and N is the total

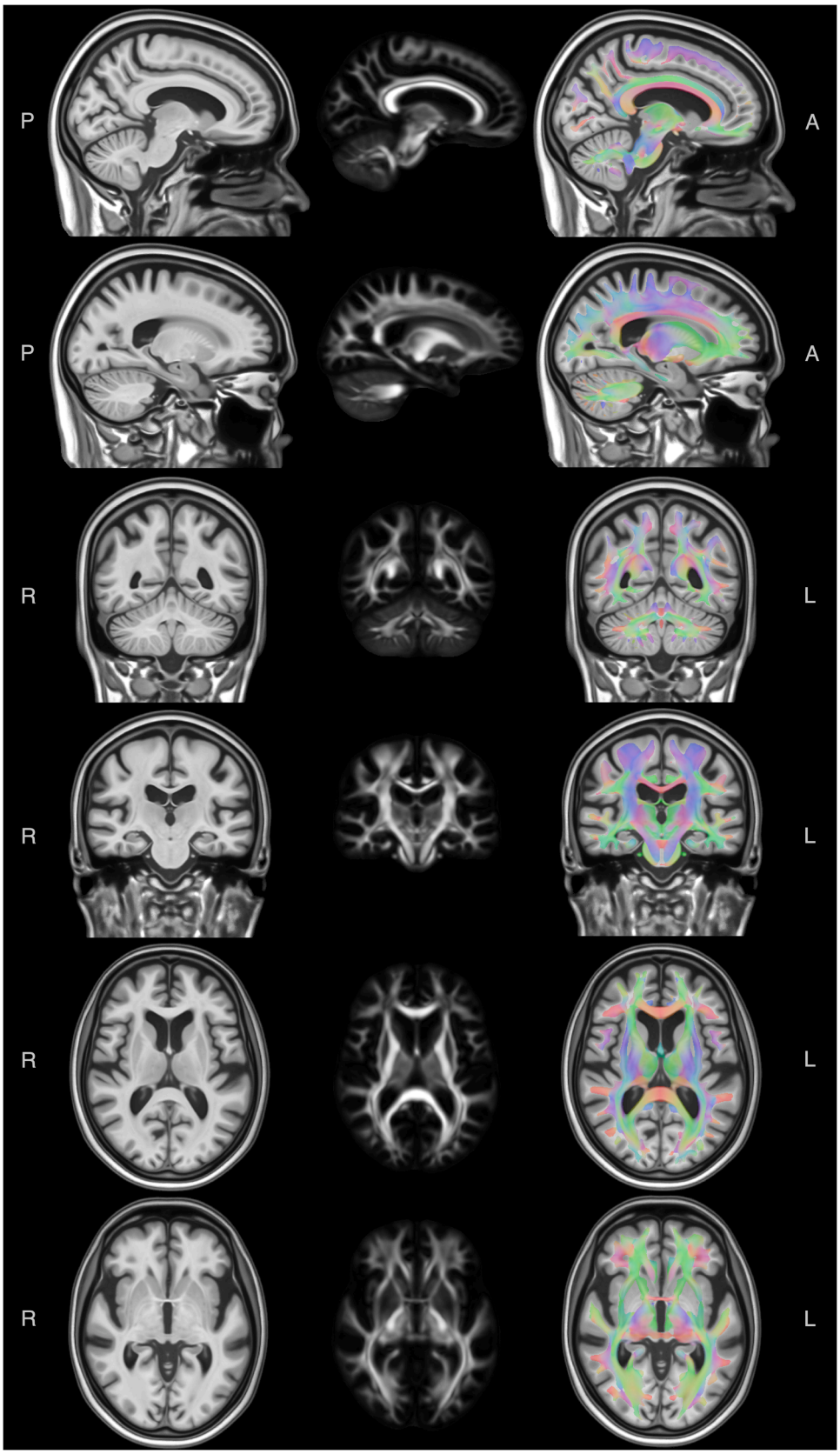

Fig. 2. Examples of sagittal, coronal and axial slices of the MIITRA-0.5mm T_1w template, FA map of the DTI template, and FA colormap overlaid on the T_1w template.

Table 1
T_1w, DTI and multimodal templates evaluated in this work.

	Name	No. of participants	Age range (years)	Voxel-size (mm^3)
T_1w template	MIITRA-0.5mm	400	64.9–98.9	0.5 × 0.5 × 0.5
	MCALT v1.4 (Schwarz et al., 2017)	202	30–92	0.5 × 0.5 × 0.5
	ICBM2009b Asym (Fonov et al., 2009, 2011)	152	18–44	0.5 × 0.5 × 0.5
	Colin27 (Aubert-Broche et al., 2006; Holmes et al., 1998)	1 (27 scans)	33	0.5 × 0.5 × 0.5
	HCP-1200 (Glasser et al., 2013)	1113	22–35	0.7 × 0.7 × 0.7
	MIITRA-1mm-2021 (Ridwan et al., 2021a)	222	65–95	1 × 1 × 1
	Oxford-MM-0 (Arthofer et al., 2021)	713	45–81	1 × 1 × 1
DTI template	MIITRA-0.5mm	400	64.9–98.9	0.5 × 0.5 × 0.5
	Oxford-MM-0 (Arthofer et al., 2021)	713	45–81	1 × 1 × 1
	ICBM81 (Mori et al., 2008)	81	18–59	1 × 1 × 1
	IXI aging v2.0 (Zhang et al., 2010)	51	65–83	1.75 × 1.75 × 2.25
Multimodal templates	MIITRA-0.5mm T_1w & DTI	400	64.9–98.9	0.5 × 0.5 × 0.5
	Oxford-MM-0 T_1w & DTI (Arthofer et al., 2021)	713	45–81	1 × 1 × 1
	MNI152 T_1w & ICBM81 DTI (Grabner et al., 2006; Mori et al., 2008)	152 / 81	18–44 / 18–59	1 × 1 × 1

number of participants of Dataset 2 (Basser and Pajevic, 2000; Jones et al., 2002). The COH was calculated in each voxel, and cumulative distributions of COH in white matter were compared across DTI templates using the one-sided two-sample Kolmogorov-Smirnov (KS) test. Differences were considered significant at $p<0.05$.

The precision of inter-modality intra-subject spatial matching achieved for T_1w and DTI data of Dataset 2 when different multimodal templates were used as reference was also evaluated. More specifically, the white matter, gray matter and ventricle masks of participants from Dataset 2 were transformed to both the T_1w template space (using the T_1w-based transformations) and the DTI template space (using the tensor-based transformations) and the Jaccard index (JI) between the two versions of the masks was calculated for each participant of Dataset 2. The average JI over all participants of Dataset 2 was compared across multimodal templates using one-way ANOVA followed by the Tukey-Kramer post-hoc test. Differences were considered significant at $p<0.05$.

2.4.2. Impact of spatial normalization precision on the ability to detect small inter-group differences

The impact of spatial normalization precision achieved with each template as reference on the ability to detect small inter-group differences was assessed using power analysis (Wicks et al., 2011; Zhang and Arfanakis, 2018; Ridwan et al., 2021a; Niaz et al., 2022). To accomplish this evaluation for the T_1w templates, the gray matter tissue probability maps from Dataset 2 were transformed to each T_1w template space using the T_1w-based transformations generated above and the resulting maps were smoothed using a Gaussian filter with sigma of 3.4 mm, following unmodulated voxel-based morphometry procedures (Good et al., 2002; Radua et al., 2014; Niaz et al., 2022). Maps of the standard deviation across smoothed maps were then used in power analyses to assess the minimum morphometric differences that can be detected in each voxel across two hypothetical groups, assuming 100 participants per group, significance at $p<0.05$, and power>0.95. Maps of the minimum detectable inter-group morphometric differences were generated for each T_1w template, and cumulative distributions were compared across T_1w templates using the one-sided two-sample Kolmogorov-Smirnov (KS) test. Differences were considered significant at $p<0.05$. A similar evaluation was conducted for the DTI templates. More specifically, the FA maps from Dataset 2 were transformed to each DTI template space using the tensor-based transformations generated in the previous section and the resulting maps were smoothed using a Gaussian filter with sigma of 3.4 mm. Maps of the standard deviation across smoothed FA maps were used in power analysis to assess the minimum detectable inter-group FA difference in each white matter voxel. Cumulative distributions of the minimum detectable inter-group FA differences were compared across DTI templates using the one-sided two-sample Kolmogorov-Smirnov (KS) test, and differences were considered significant at $p<0.05$.

2.4.3. Evaluation of templates in terms of their representativeness of the brain of non-demented older adults

The representativeness of the brain of non-demented older adults was assessed for each template in terms of the average log-Jacobian determinant of the deformations performed for spatial normalization of Dataset 2 when each template is used as reference. The log-Jacobian determinant is used in each voxel as a local index of volume change during spatial normalization, indicating tissue expansion (log-Jacobian determinant > 0) or shrinkage (log-Jacobian determinant < 0) (Chung et al., 2001; Leow et al., 2007; Yanovsky et al., 2009). For the evaluation of T_1w templates, maps of log-Jacobian determinant were generated from deformations of T_1w images from Dataset 2 to the T_1w templates and were averaged over all participants transformed to the same space. Histograms of the average log-Jacobian determinant were compared across T_1w templates using a one-sided two-sample Kolmogorov-Smirnov (KS) test, separately for expansion and shrinkage. Differences were considered significant at $p<0.05$. The same approach was used to compare DTI templates in terms of their representativeness of the older adult brain.

3. Results

3.1. T_1w and DTI template image quality

Visual inspection of the new MIITRA-0.5mm T_1w and DTI templates showed that major structures of the cerebrum, cerebellum, and brainstem, cortical and subcortical gray matter, white matter, ventricles, gyri and sulci were well-defined and free of artifacts, fine structures were well-resolved (e.g. cortex of the cerebellum, anterior commissure), and brain T_1w and DTI features were well-matched in space (Fig. 2). Quantitative comparison of the normalized power spectra showed higher energy at high spatial frequencies in all three axes for the MIITRA-0.5mm T_1w template compared to other standardized T_1w templates, indicating higher image sharpness for the MIITRA-0.5mm T_1w template (Fig. 3). The FA map of the new MIITRA-0.5mm DTI template is also characterized by higher image sharpness compared to other standardized DTI templates as demonstrated in the normalized power spectra (Fig. 4).

3.2. Comparison of templates in terms of inter-subject and inter-modality spatial normalization precision of older adult data

In terms of the intra-modality inter-subject spatial normalization

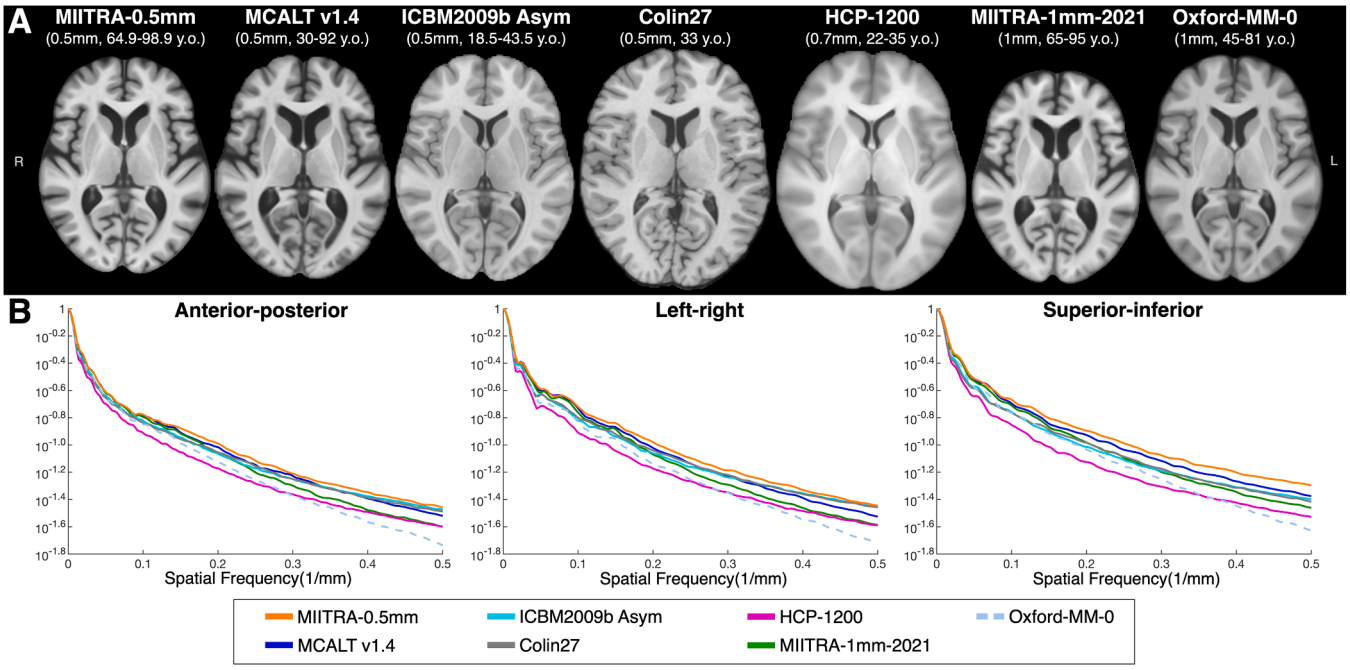

Fig. 3. (A) Axial slices of the MIITRA-0.5mm, MCALT v1.4, ICBM2009b Asym, Colin27, HCP-1200, MIITRA-1mm-2021, and Oxford-MM-0 T_1w templates. (B) Normalized power spectra for the anterior-posterior (AP), left-right (LR), and superior-inferior (SI) axes of all T_1w templates. The energy at high spatial frequencies in the normalized power spectra was higher for MIITRA-0.5mm compared to other T_1w templates.

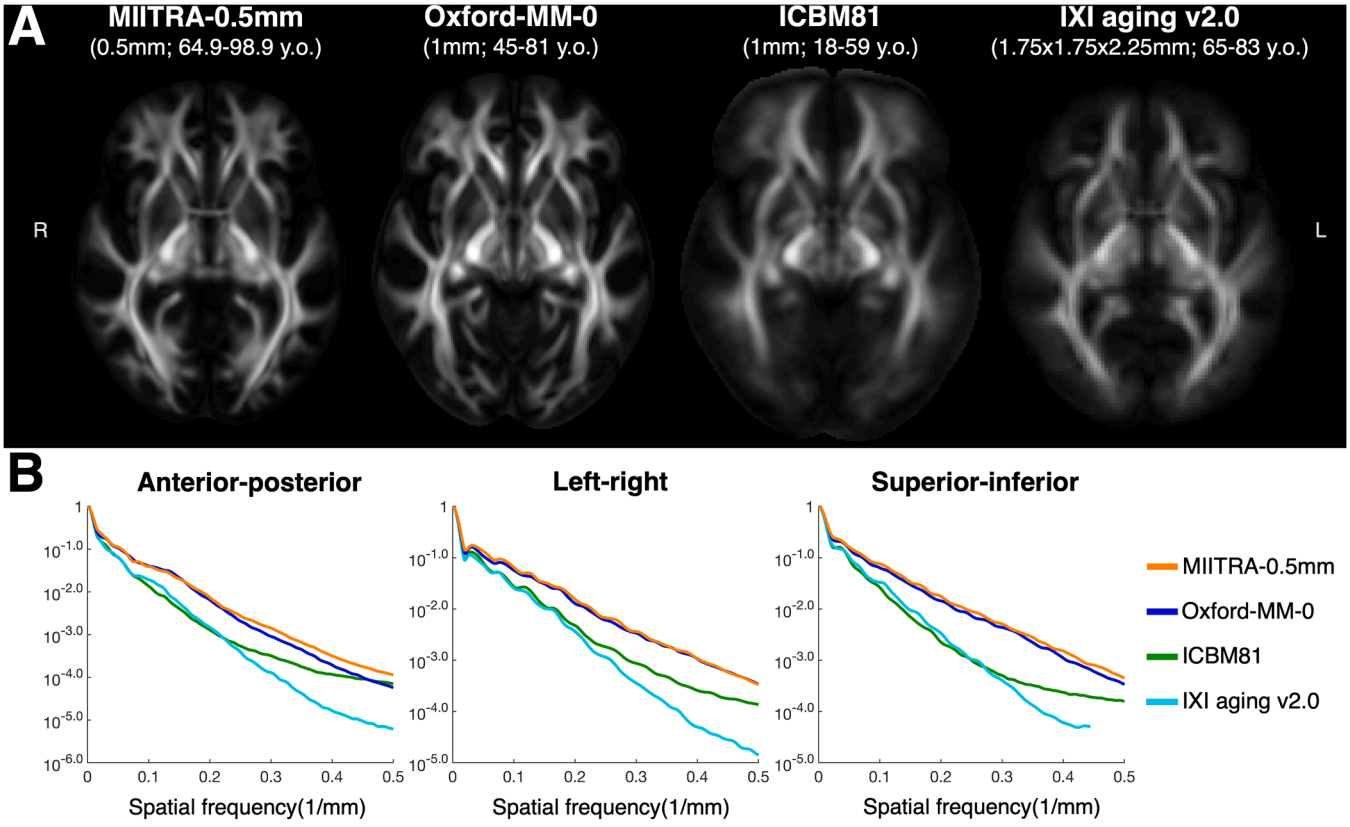

Fig. 4. (A) Axial slices of FA maps of the MIITRA-0.5mm, Oxford-MM-0, ICBM81 and IXI aging v2.0 DTI templates. (B) Normalized power spectra for the anterior-posterior (AP), left-right (LR), and superior-inferior (SI) axes of all of FA templates. The energy at high spatial frequencies in the normalized power spectra of FA maps from MIITRA-0.5mm was higher compared to other DTI templates.

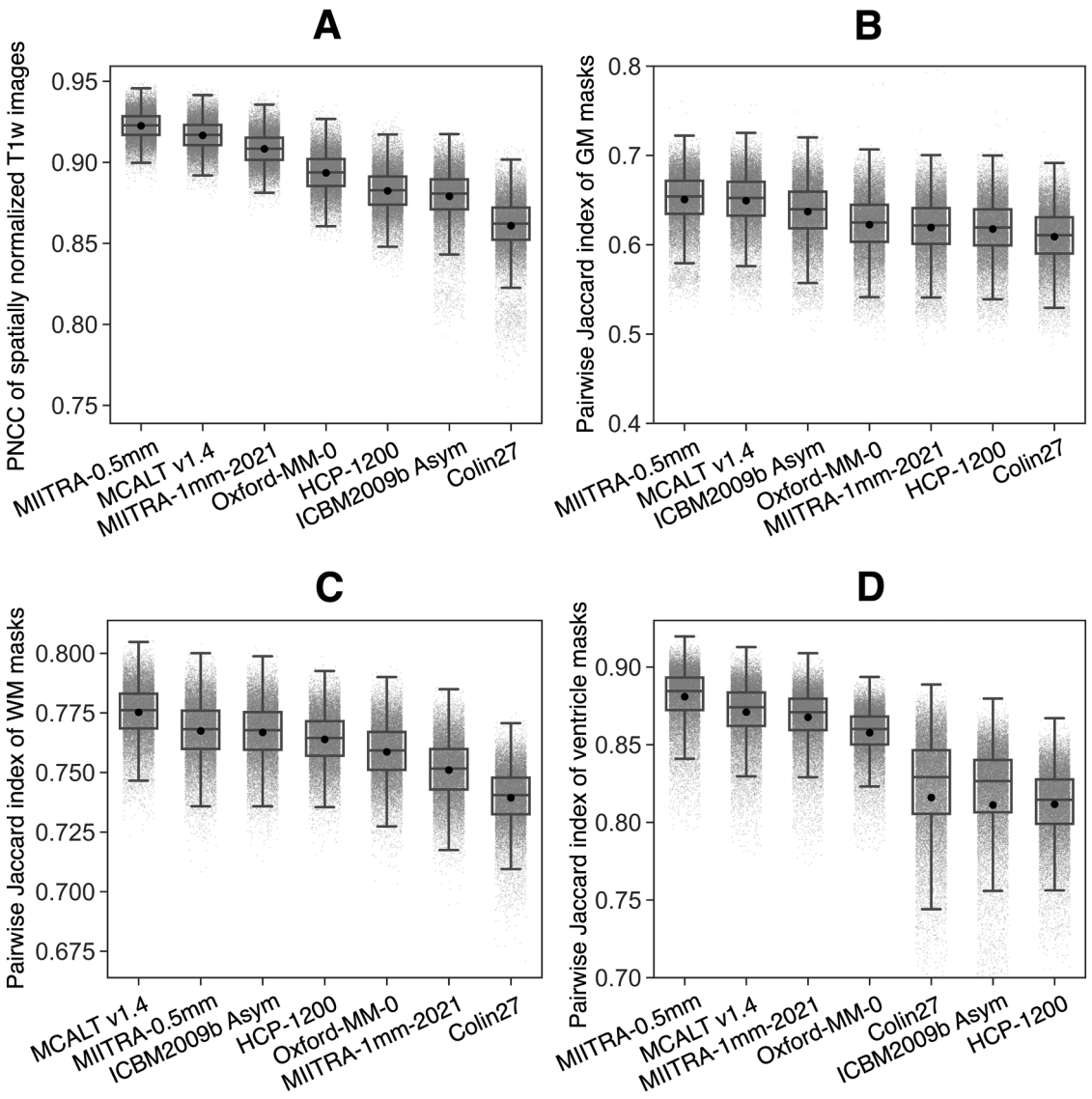

Fig. 5. Boxplots of the (A) pairwise normalized cross-correlation (PNCC), (B) pairwise Jaccard index (JI) of gray matter masks, (C) pairwise JI of white matter masks, and (D) pairwise JI of ventricle masks from spatially normalized older adult T_1w images of Dataset 2 when using different T_1w templates as references.

precision achieved for T_1w data from Dataset 2 when using different templates as reference, the MIITRA-0.5mm T_1w template resulted in higher average PNCC of normalized T_1w data ($p<0.05$) (Fig. 5A), higher average pairwise JI of normalized gray matter masks ($p<0.05$) (Fig. 5B), the second highest average pairwise JI of normalized white matter masks ($p<0.05$), and higher average pairwise JI of ventricle masks

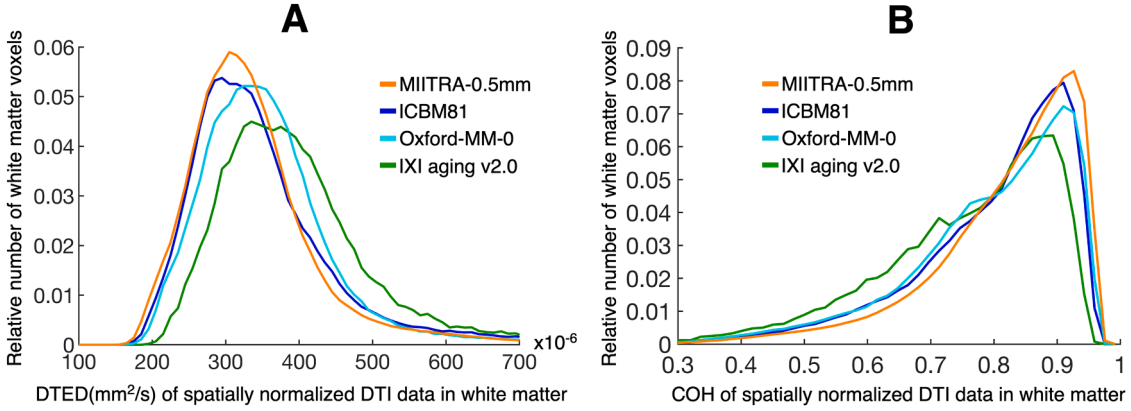

Fig. 6. Histograms of the relative number of white matter voxels at different values of (A) average pairwise Euclidean distance of tensors (DTED) and (B) coherence of primary eigenvectors (COH) across spatially normalized older adult DTI data of Dataset 2 when using different DTI templates as references.

($p<0.05$) (Fig. 5D) compared to all other T_1w templates. These findings demonstrate that the MIITRA-0.5mm T_1w template provided higher inter-subject spatial normalization precision for older adult T_1w data from Dataset 2 compared to other templates especially in gray matter and the ventricles.

In terms of the intra-modality inter-subject spatial normalization precision achieved for DTI data from Dataset 2 when using different templates as reference, the MIITRA-0.5mm DTI template resulted in a higher number of white matter voxels with lower DTED ($p<10^{-10}$) (Fig. 6A), and a higher number of white matter voxels with higher COH ($p<10^{-10}$) (Fig. 6B) compared to all other DTI templates. These results demonstrate that the MIITRA-0.5mm DTI template provided higher inter-subject spatial normalization precision for older adult DTI data from Dataset 2 compared to other templates.

In terms of the inter-modality intra-subject spatial matching achieved for T_1w and DTI data of Dataset 2 when different multimodal templates are used as reference, the MIITRA-0.5mm T_1w and DTI templates resulted in higher average JI between white matter masks transformed to template space using T_1w transformations and the same masks transformed to template space using DTI transformations, compared to all other multimodal templates ($p<0.05$) (Fig. 7). The same was true for gray matter masks and ventricle masks. These findings demonstrate that the MIITRA-0.5mm T_1w and DTI templates provided higher inter-modality intra-subject spatial matching for older adult data from Dataset 2 compared to other multimodal templates.

3.3. Impact of spatial normalization precision on the ability to detect small inter-group differences

Power analysis showed that use of the MIITRA-0.5mm T_1w template as a reference for spatial normalization of older adult T_1w data allows detection of smaller inter-group morphometric differences in gray matter, compared to other T_1w templates. This was demonstrated in Fig. 8A as a higher number of gray matter voxels with cooler colors and a lower number of voxels with warmer colors when using the MIITRA-0.5mm T_1w template. Also, the cumulative distribution of the minimum detectable inter-group morphometric differences was significantly shifted to the left for the MIITRA-0.5mm T_1w template compared to other T_1w templates ($p<10^{-10}$ in all cases) (Fig. 8B).

A separate power analysis showed that use of the MIITRA-0.5mm DTI template as a reference for spatial normalization of older adult DTI data allows detection of smaller inter-group FA differences in white matter, compared to other DTI templates. This was demonstrated in Fig. 9A as a higher number of white matter voxels with cooler colors and a lower number of voxels with warmer colors when using the MIITRA-0.5mm DTI template (Fig. 9A). Also, the cumulative distribution of the minimum detectable inter-group FA differences was significantly shifted to the left for the MIITRA-0.5mm DTI template compared to other DTI templates ($p<10^{-10}$ in all cases) (Fig. 9B).

3.4. Comparison of templates in terms of their representativeness of the brain of non-demented older adults

When registering older adult T_1w data from Dataset 2 to the MIITRA-0.5mm T_1w template a higher number of voxels exhibited an average log-Jacobian determinant near zero compared to registration to other high resolution T_1w templates, namely MCALT v1.4, ICBM2009b Asym, Colin27 and HCP-1200 ($p<10^{-10}$ in both expansion and contraction) (Fig. 10). This suggests that MIITRA-0.5mm T_1w template is more representative of the older adult T_1w data of Dataset 2 than other high resolution templates. Only the lower resolution templates (MIITRA-1mm-2021 and Oxford-MM-0) resulted in less deformation ($p<10^{-10}$) because their larger voxels limit local deformations (not a fair comparison). Among DTI templates, MIITRA-0.5mm was the only high resolution DTI template, yet it required lower average deformation of older adult data than even the lower resolution ICBM81 and IXI v2.0 DTI templates ($p<10^{-10}$ in both expansion and contraction) (Fig. 11). Only Oxford-MM-0 DTI template required even less deformation ($p<10^{-10}$) but again templates with larger voxels limit local deformations (not a fair comparison). These findings suggest that MIITRA-0.5mm DTI template is representative of the non-demented older adult data of Dataset 2.

4. Discussion

The present work constructed high quality 0.5 mm isotropic resolution multimodal T_1w and DTI templates of the brain of non-demented older adults in a common space using advanced multimodal template construction techniques and principles of super resolution on data from a large, diverse, community cohort of 400 non-demented older adults. It was demonstrated that the new MIITRA-0.5mm T_1w and DTI templates are well-matched in space, exhibit good definition of brain structures, including fine structures, exhibit higher image sharpness than other standardized templates, and are free of artifacts, all essential prerequisites for precise spatial normalization when used as references. Indeed, the MIITRA-0.5mm T_1w and DTI templates allowed higher intra-modality inter-subject spatial normalization precision as well as higher inter-modality intra-subject spatial matching of non-demented older adult T_1w and DTI data compared to other available standardized

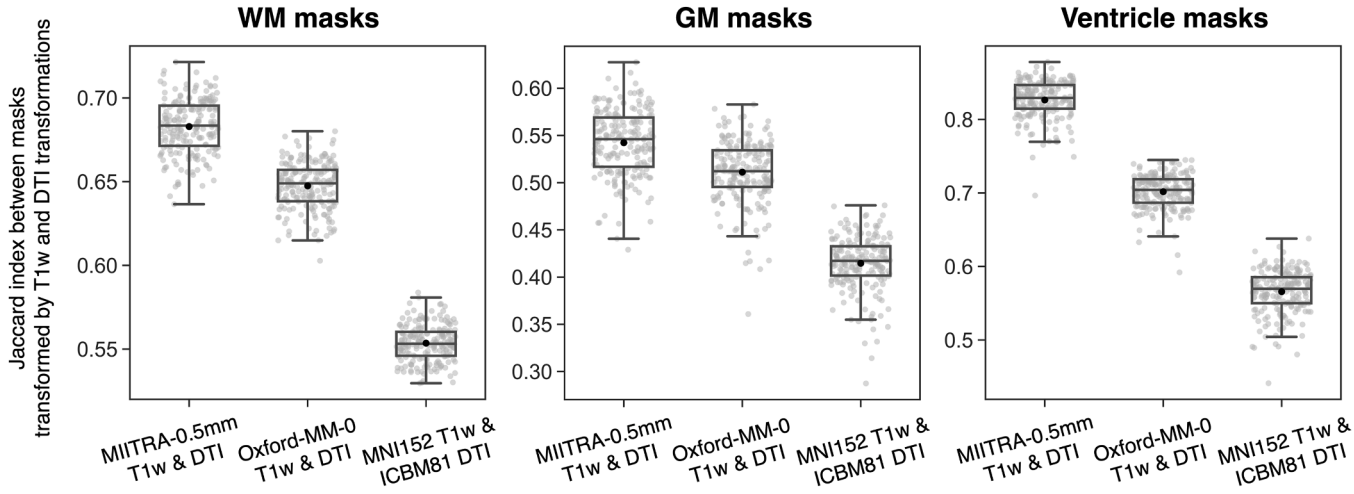

Fig. 7. Boxplots of the Jaccard index (JI) between older adult white matter/gray matter/ventricle masks of Dataset 2 transformed to the space of multimodal templates using T_1w transformations and the same masks transformed to template space using DTI transformations.

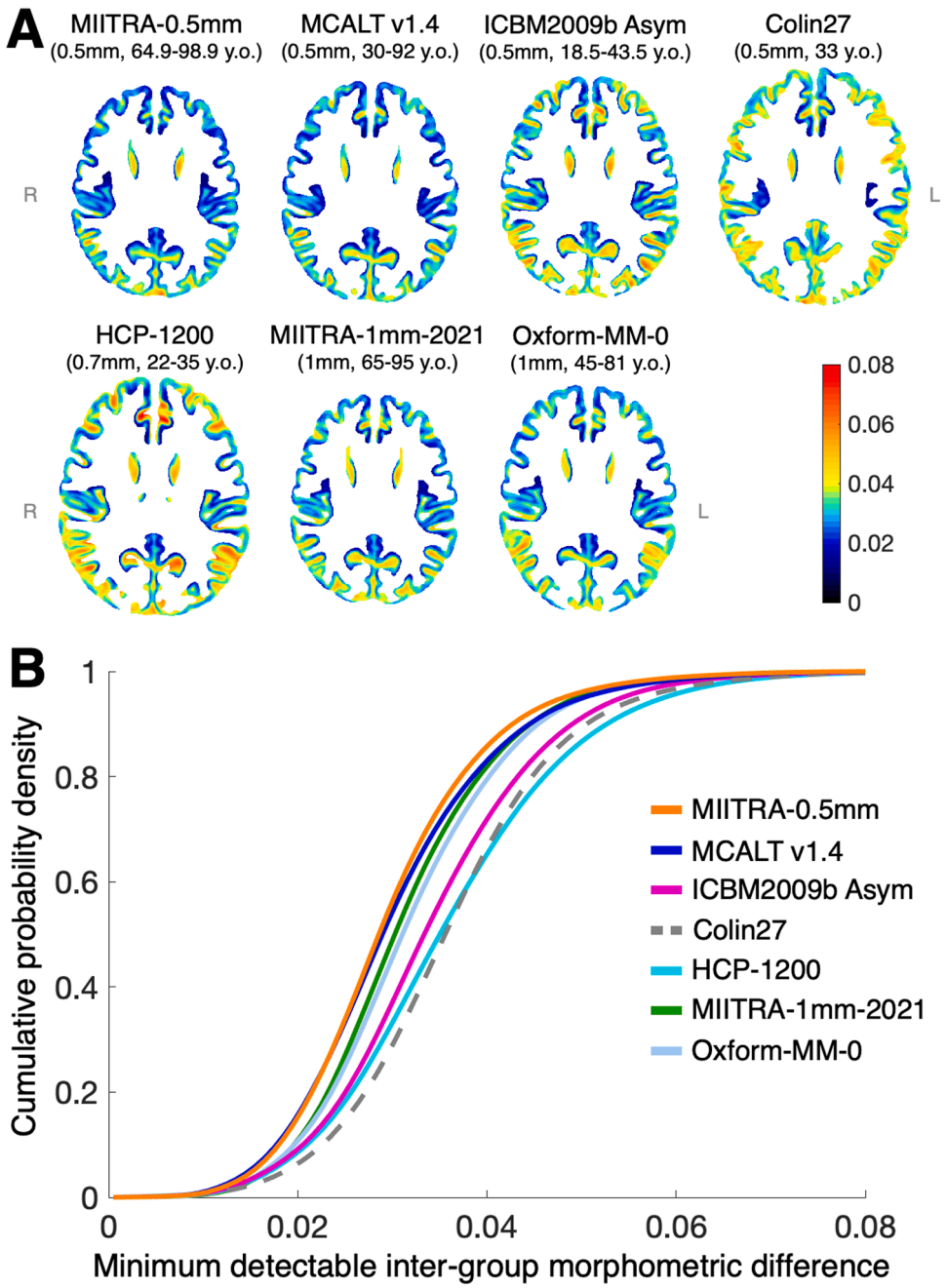

Fig. 8. (A) Maps and (B) cumulative distributions of the minimum detectable inter-group morphometric differences in gray matter when using different T_1w templates as references, according to a power analysis in older adult T_1w data from Dataset 2.

templates. Consequently, MIITRA-0.5mm templates allowed detection of smaller inter-group differences for older adult data compared to other templates. Lastly, the MIITRA-0.5mm templates were shown to be most representative of the brain of non-demented older adults compared to other templates with submillimeter resolution. The new templates constructed in this work constitute two of the final products of the MIITRA atlas project and are anticipated to have important implications for the sensitivity and precision of studies on older adults. They are available for download at www.nitrc.org/projects/miitra.

In MIITRA-0.5mm T_1w and DTI templates, major structures of the older adult brain were well-defined and free of artifacts, fine structures were well-resolved, image sharpness was higher than that of other standardized templates, and brain T_1w and DTI features were well-matched in space. A number of factors led to these characteristics. Using good quality raw data in combination with a state-of-the-art iterative multimodal template construction approach resulted in precise spatial alignment of the raw data across participants reducing blurring, as well as in precise spatial alignment across modalities enhancing spatial matching of the final templates (Wu et al., 2022). Combining all transformations into one, forward mapping signals from raw space to exact physical locations in template space, and applying multiple image super resolution principles minimized interpolations thereby further reducing blurring, and revealed fine brain details (Niaz et al., 2022). The use of a patch-based sparse representation data fusion technique instead of simple averaging also reduced blurring by diminishing the contribution of any misregistered structures to the final templates (Ridwan et al., 2021b; Shi et al., 2014) (Appendix 1 generated a 0.5 mm T_1w template ignoring most of the above steps of the template construction approach and demonstrates the important value of these steps). Overall, the approach used in this work resulted in multimodal

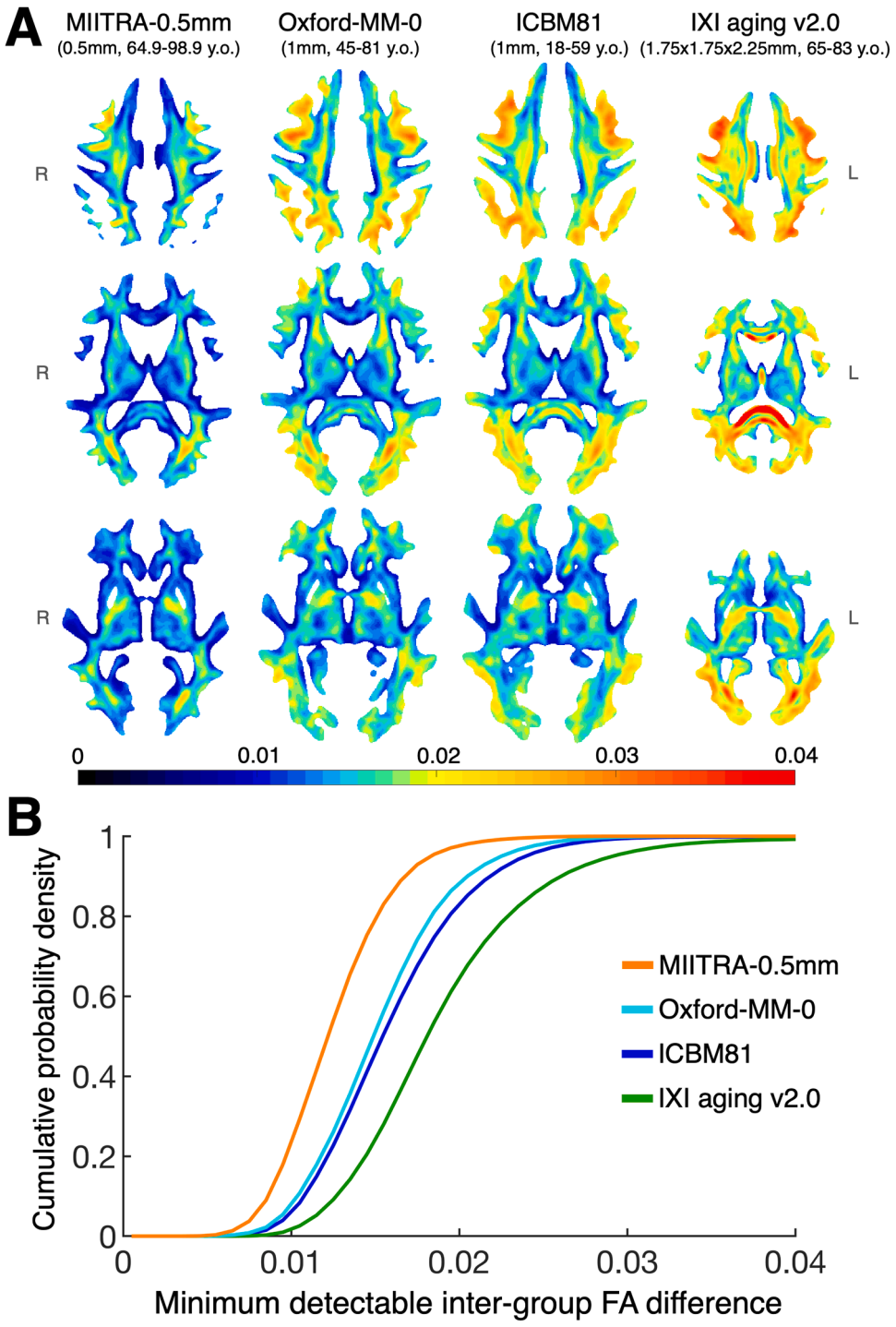

Fig. 9. (A) Maps and (B) cumulative distributions of the minimum detectable inter-group FA differences in white matter when using different DTI templates as references, according to a power analysis in older adult DTI data from Dataset 2.

templates possessing characteristics that are important for precise inter-subject and inter-modality spatial normalization of older adult data when these templates are used as references.

As expected, the MIITRA-0.5mm T_1w and DTI templates provided higher intra-modality inter-subject spatial normalization precision as well as higher inter-modality intra-subject spatial matching of non-demented older adult T_1w and DTI data compared to other available standardized templates. The same conclusion can be extended for the performance of the MIITRA-0.5mm T_1w template in comparison to several other available T_1w templates that were not considered here, because MIITRA-0.5mm outperformed MIITRA-1mm-2021 which was recently shown to outperform approximately 20 other known templates (see Ridwan et al., 2021a). By providing higher spatial normalization precision, the MIITRA-0.5mm T_1w and DTI templates can lower variability in univariate and multivariate voxel-wise analyses, thereby enhancing the sensitivity and specificity of neuroimaging studies of the older adult brain (Hsu et al., 2015; Ridwan et al., 202la; Zhang and Arfanakis, 2018). Direct evidence of this was the finding that the MIITRA-0.5mm templates allowed detection of smaller inter-group differences compared to other templates. Detecting small brain changes

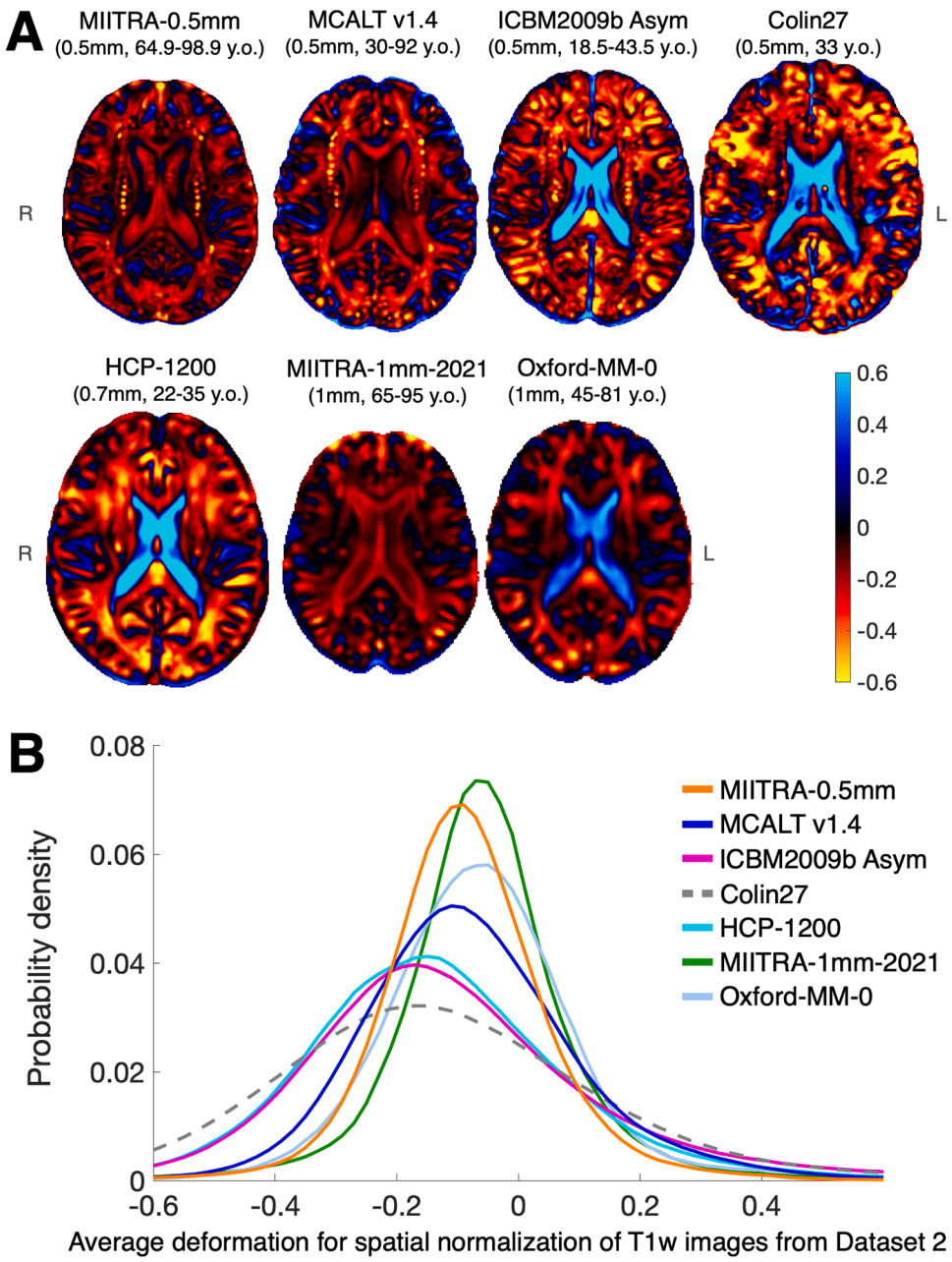

Fig. 10. (A) Maps and (B) histograms of the average log-Jacobian determinant of the deformation of older adult T_1w images from Dataset 2 for registration to different T_1w templates.

and doing so at submillimeter resolution is of particular interest in studies of aging as early brain abnormalities are naturally small, and for several devastating age-related diseases these abnormalities begin in small-sized brain structures.

The MIITRA-0.5mm T_1w and DTI templates were more representative of the brain of non-demented older adults than other high resolution templates. This was due to the large, diverse, community cohort of exclusively older adults that the new templates are based on, the construction of an initial unbiased template which helped to avoid bias to any individual anatomy or pre-selected template, and in general due to the iterative multimodal template construction approach used. Several of the other templates were built using not only data on older adults but also data on middle-aged and young adults and were therefore naturally less representative of the older adult brain, requiring larger deformations for spatial normalization of older adult data. This finding is important for studies of the older adult brain because use of a representative template can enhance image registration and increase the accuracy of downstream quantification and analysis (Fonov et al., 2011; Good et al., 2001; Senjem et al., 2005; Yoon et al., 2009). Finally, it should be stressed here that the amount of deformation required for spatial normalization can only be compared across templates of the same resolution as templates with larger voxels limit local deformations by default and therefore a comparison across resolutions is not meaningful.

In addition to the multiple strengths of the present work, there are also a few caveats. First, the template construction process used for the development of the MIITRA-0.5mm T_1w and DTI templates is computationally expensive and time consuming. However, since the MIITRA-0.5mm templates are standardized i.e. constructed only once and made available for use in multiple studies, no further investment of resources or time is needed. Second, the performance of the MIITRA-0.5mm T_1w template was compared to only 6 other popular templates while several other T_1w templates have been developed over the last two

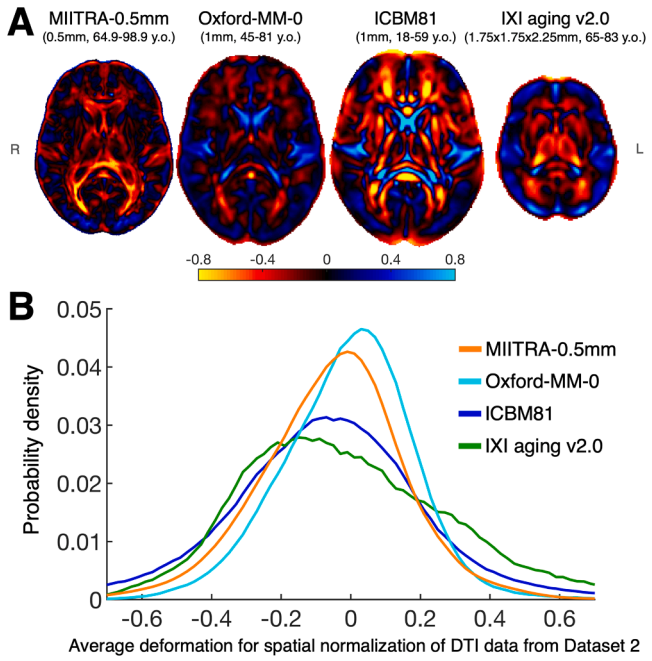

Fig. 11. (A) Maps and (B) histograms of the average log-Jacobian determinant of the deformation of older adult DTI data from Dataset 2 for registration to different DTI templates.

decades. However, an exhaustive comparison recently demonstrated that MIITRA-1mm-2021 had superior performance than several other templates (Ridwan et al., 2021a), and in the present work MIITRA-0.5mm outperformed MIITRA-1mm-2021, therefore it is not necessary to duplicate those comparisons. Third, the T_1w and DTI data utilized for template construction did not have 0.5 mm isotropic resolution because such data is currently unavailable due to obvious technical limitations that are accentuated when it comes to imaging a large number of older adults. The same limitation is true however for all other available 0.5 mm isotropic resolution templates. Fourth, even though the cohort that participated in the construction of the MIITRA templates was more diverse than that of other popular templates (e.g. the sample in ICBM2009b was ~90% white) diversity needs to be further enhanced in our sample and efforts are underway to do exactly that (especially for Latino and Asian representation). Finally, in the present study spatial normalization was evaluated using state-of-the-art registration algorithms and older adult data of typical quality for studies of aging. Future work should consider other registration algorithms as well as data with different image quality.

5. Conclusion

The new MIITRA-0.5mm T_1w and DTI templates are of high quality, have submillimeter resolution, and were constructed in a common space using advanced multimodal template construction techniques and principles of super resolution on data from a large, diverse, community cohort of non-demented older adults. The new MIITRA-0.5mm templates allowed higher inter-subject and inter-modality spatial matching of non-demented older adult T_1w and DTI data compared to other available templates. Thus, MIITRA-0.5mm allowed detection of smaller inter-group differences for older adult data compared to other templates. Furthermore, the MIITRA-0.5mm templates were shown to be most representative of the brain of non-demented older adults compared to other templates with submillimeter resolution. The new templates constructed in this work constitute two of the final products of the MIITRA atlas project and are anticipated to have important implications for the sensitivity and precision of studies on older adults.

Funding

This study was supported by National Institute on Aging (NIA) grants R01AG052200, P30AG010161, P30AG072975, R01AG017917, R01AG022018, R01AG056405, R01AG015819, R01AG064233 and National Institute of Neurological Disorders and Stroke (NINDS) grant UF1NS100599.

In addition, part of the data collection and sharing for this project was funded by the Alzheimer's Disease Neuroimaging Initiative (ADNI) (National Institutes of Health Grant U01 AG024904) and DOD ADNI (Department of Defense award number W81XWH-12–2–0012). ADNI is funded by the National Institute on Aging, the National Institute of Biomedical Imaging and Bioengineering, and generous contributions from the following: AbbVie; Alzheimer's Association; Alzheimer's Drug Discovery Foundation; Araclon Biotech; BioClinica, Inc.; Biogen; Bristol-Myers Squibb Company; CereSpir, Inc.; Cogstate; Eisai; Elan Pharmaceuticals, Inc.; Eli Lilly and Company; EuroImmun; F. Hoffmann-La Roche and its affiliated company Genentech, Inc.; Fujirebio; GE Healthcare; IXICO Ltd.; Janssen Alzheimer Immunotherapy Research & Development, LLC.; Johnson & Johnson Pharmaceutical Research & Development LLC.; Lumosity; Lundbeck; Merck & Co., Inc.; Meso Scale Diagnostics, LLC.; NeuroRx Research; Neurotrack Technologies; Novartis Pharmaceuticals Corporation; Pfizer Inc.; Piramal Imaging; Servier; Takeda Pharmaceutical Company; and Transition Therapeutics. The Canadian Institutes of Health Research is providing funds to support ADNI clinical sites in Canada. Private sector contributions are facilitated by the Foundation for the National Institutes of Health (www.fnih.org/). The grantee organization is the Northern California Institute for Research and Education, and the study is coordinated by the Alzheimer's Therapeutic Research Institute at the University of Southern California. ADNI data are disseminated by the Laboratory for Neuro Imaging at the University of Southern California.

Data and template availability statement

The data used in this work can be assessed by submitting a request to www.radc.rush.edu. The new templates are available for download at www.nitrc.org/projects/miitra.

CRediT authorship contribution statement

Yingjuan Wu: Conceptualization, Methodology, Software, Validation, Formal analysis, Investigation, Data curation, Writing – original draft, Writing – review & editing, Visualization. **Abdur Raquib Ridwan:** Conceptualization, Methodology, Software, Validation, Formal analysis, Investigation, Data curation, Writing – original draft, Writing – review & editing, Visualization. **Mohammad Rakeen Niaz:** Conceptualization, Methodology, Software, Validation, Investigation, Data curation, Writing – original draft, Writing – review & editing. **David A. Bennett:** Resources, Data curation, Writing – review & editing, Funding acquisition. **Konstantinos Arfanakis:** Conceptualization, Methodology, Validation, Formal analysis, Investigation, Resources, Data curation, Writing – original draft, Writing – review & editing, Visualization, Supervision, Project administration, Funding acquisition.

Declaration of Competing Interest

The authors have no conflict of interest to report.

Data availability

Data will be made available on request.

Acknowledgements

The authors would like to thank the participants and staff of the Rush Memory and Aging Project, Religious Orders Study, Minority Aging Research Study, Clinical Core and Latino Core of the Rush Alzheimer's Disease Research Center, and the Alzheimer's Disease Neuroimaging Initiative.

Supplementary materials

Supplementary material associated with this article can be found, in the online version, at doi:10.1016/j.neuroimage.2023.120387.

References

Alexander, D.C., Gee, J.C., 2000. Elastic matching of diffusion tensor images. Comp. Vision Image Understan. 77 (2), 233–250.

Ardekani, B.A., Bachman, A.H., 2009. Model-based automatic detection of the anterior and posterior commissures on MRI scans. Neuroimage 46 (3), 677–682. https://doi.org/10.1016/j.neuroimage.2009.02.030.

Arthofer, C., Smith, S.M., Jenkinson, M., Andersson, J., Lange, F., 2021. Multimodal MRI Template Construction from UK Biobank: Oxford-MM-0. Organisation for Human Brain Mapping (OHBM).

Aubert-Broche, B., Evans, A.C., Collins, L., 2006. A new improved version of the realistic digital brain phantom. Neuroimage 32 (1), 138–145. https://doi.org/10.1016/j.neuroimage.2006.03.052.

Avants, B., Duda, J.T., Kim, J., Zhang, H., Pluta, J., Gee, J.C., Whyte, J., 2008a. Multivariate analysis of structural and diffusion imaging in traumatic brain injury. Acad. Radiol. 15 (11), 1360–1375. https://doi.org/10.1016/j.acra.2008.07.007.

Avants, B.B., Cook, P.A., Ungar, L., Gee, J.C., Grossman, M., 2010a. Dementia induces correlated reductions in white matter integrity and cortical thickness: a multivariate neuroimaging study with sparse canonical correlation analysis. Neuroimage 50 (3), 1004–1016. https://doi.org/10.1016/j.neuroimage.2010.01.041.

Avants, B.B., Epstein, C.L., Grossman, M., Gee, J.C., 2008b. Symmetric diffeomorphic image registration with cross-correlation: evaluating automated labeling of elderly and neurodegenerative brain. Med. Image Anal. 12 (1), 26–41. https://doi.org/10.1016/j.media.2007.06.004.

Avants, B.B., Tustison, N., Song, G., 2009. Advanced normalization tools (ANTS). Insight J 2 (365), 1–35.

Avants, B.B., Tustison, N.J., Song, G., Cook, P.A., Klein, A., Gee, J.C., 2011. A reproducible evaluation of ANTs similarity metric performance in brain image registration. Neuroimage 54 (3), 2033–2044. https://doi.org/10.1016/j.neuroimage.2010.09.025.

Avants, B.B., Yushkevich, P., Pluta, J., Minkoff, D., Korczykowski, M., Detre, J., Gee, J.C., 2010b. The optimal template effect in hippocampus studies of diseased populations. Neuroimage 49 (3), 2457–2466. https://doi.org/10.1016/j.neuroimage.2009.09.062.

Barnes, L.L., Shah, R.C., Aggarwal, N.T., Bennett, D.A., Schneider, J.A., 2012. The minority aging research study: ongoing efforts to obtain brain donation in African Americans without dementia. Curr. Alzheimer Res 9 (6), 734–745. https://doi.org/10.2174/156720512801322627.

Basser, P.J., Pajevic, S., 2000. Statistical artifacts in diffusion tensor MRI (DT-MRI) caused by background noise. Magn. Reson. Med. 44 (1), 41–50. https://doi.org/10.1002/1522-2594(200007)44:1<41::aid-mrm8>3.0.co;2-o.

Bennett, D.A., Buchman, A.S., Boyle, P.A., Barnes, L.L., Wilson, R.S., Schneider, J.A., 2018. Religious Orders Study and Rush Memory and Aging Project. JAD 64 (s1), S161–S189. https://doi.org/10.3233/JAD-179939.

Blatter, D.D., Bigler, E.D., Gale, S.D., Johnson, S.C., Anderson, C.V., Burnett, B.M., Parker, N., Kurth, S., Horn, S.D., 1995. Quantitative volumetric analysis of brain MR: normative database spanning 5 decades of life. AJNR Am. J. Neuroradiol 16 (2), 241–251.

Bookheimer, S.Y., Salat, D.H., Terpstra, M., Ances, B.M., Barch, D.M., Buckner, R.L., Burgess, G.C., Curtiss, S.W., Diaz-Santos, M., Elam, J.S., Fischl, B., Greve, D.N., Hagy, H.A., Harms, M.P., Hatch, O.M., Hedden, T., Hodge, C., Japardi, K.C., Kuhn, T. P., Ly, T.K., Yacoub, E., 2019. The lifespan human connectome project in aging: an overview. Neuroimage 185, 335–348. https://doi.org/10.1016/j.neuroimage.2018.10.009.

Calhoun, V.D., Sui, J., 2016. Multimodal fusion of brain imaging data: a key to finding the missing link(s) in complex mental illness. Biol. Psych. Cogn. Neurosci. Neuroimaging (1), 230–244. https://doi.org/10.1016/j.bpsc.2015.12.005.

Chang, L.C., Jones, D.K., Pierpaoli, C., 2005. RESTORE: robust estimation of tensors by outlier rejection. Magn. Reson. Med. 53 (5), 1088–1095. https://doi.org/10.1002/mrm.20426.

Chang, L.C., Walker, L., Pierpaoli, C., 2012. Informed RESTORE: a method for robust estimation of diffusion tensor from low redundancy datasets in the presence of physiological noise artifacts. Magn. Reson. Med. 68 (5), 1654–1663. https://doi.org/10.1002/mrm.24173.

Chung, M.K., Worsley, K.J., Paus, T., Cherif, C., Collins, D.L., Giedd, J.N., Rapoport, J.L., Evans, A.C., 2001. A unified statistical approach to deformation-based morphometry. Neuroimage 14 (3), 595–606. https://doi.org/10.1006/nimg.2001.0862.

Cox, S.R., Ritchie, S.J., Tucker-Drob, E.M., Liewald, D.C., Hagenaars, S.P., Davies, G., Wardlaw, J.M., Gale, C.R., Bastin, M.E., Deary, I.J., 2016. Ageing and brain white matter structure in 3,513 UK Biobank participants. Nat. Commun. 7, 13629. https://doi.org/10.1038/ncomms13629.

Evans, A.C., Janke, A.L., Collins, D.L., Baillet, S., 2012. Brain templates and atlases. Neuroimage 62 (2), 911–922. https://doi.org/10.1016/j.neuroimage.2012.01.024.

Farokhian, F., Beheshti, I., Sone, D., Matsuda, H., 2017. Comparing CAT12 and VBM8 for detecting brain morphological abnormalities in temporal lobe epilepsy. Front. Neurol 8, 428. https://doi.org/10.3389/fneur.2017.00428.

Ferreira, J.R., Oliveira, M.C., Freitas, A.L., 2014. Performance evaluation of medical image similarity analysis in a heterogeneous architecture. In: 2014 IEEE 27th International Symposium on Computer-Based Medical Systems. IEEE, pp. 159–164.

Fischl, B., 2012. FreeSurfer. Neuroimage 62 (2), 774–781. https://doi.org/10.1016/j.neuroimage.2012.01.021.

Fonov, V., Evans, A.C., Botteron, K., Almli, C.R., McKinstry, R.C., Collins, D.L., Brain Development Cooperative Group, 2011. Unbiased average age-appropriate atlases for pediatric studies. Neuroimage 54 (1), 313–327. https://doi.org/10.1016/j.neuroimage.2010.07.033.

Fonov, V., Evans, A., McKinstry, R., Almli, C., Collins, D., 2009. Unbiased nonlinear average age-appropriate brain templates from birth to adulthood. Neuroimage 47, S102. https://doi.org/10.1016/s1053-8119(09)70884-5.

Ge, Y., Grossman, R.I., Babb, J.S., Rabin, M.L., Mannon, L.J., Kolson, D.L., 2002. Age-related total gray matter and white matter changes in normal adult brain. Part I: volumetric MR imaging analysis. AJNR Am. J. Neuroradiol 23 (8), 1327–1333.

Glasser, M.F., Sotiropoulos, S.N., Wilson, J.A., Coalson, T.S., Fischl, B., Andersson, J.L., Xu, J., Jbabdi, S., Webster, M., Polimeni, J.R., Van Essen, D.C., Jenkinson, M., Consortium, WU-Minn HCP, 2013. The minimal preprocessing pipelines for the Human Connectome Project. Neuroimage 80, 105–124. https://doi.org/10.1016/j.neuroimage.2013.04.127.

Good, C.D., Johnsrude, I.S., Ashburner, J., Henson, R.N., Friston, K.J., Frackowiak, R.S., 2001. A voxel-based morphometric study of ageing in 465 normal adult human brains. Neuroimage 14 (1 Pt 1), 21–36. https://doi.org/10.1006/nimg.2001.0786.

Good, C.D., Scahill, R.I., Fox, N.C., Ashburner, J., Friston, K.J., Chan, D., Crum, W.R., Rossor, M.N., Frackowiak, R.S., 2002. Automatic differentiation of anatomical patterns in the human brain: validation with studies of degenerative dementias. Neuroimage 17 (1), 29–46. https://doi.org/10.1006/nimg.2002.1202.

Grabner, G., Janke, A.L., Budge, M.M., Smith, D., Pruessner, J., Collins, D.L., 2006. Symmetric atlasing and model based segmentation: an application to the hippocampus in older adults. In: Medical image computing and computer-assisted intervention: MICCAI . International Conference on Medical Image Computing and Computer-Assisted Intervention, 9, pp. 58–66. https://doi.org/10.1007/11866763_8.

Gupta, V., Malandain, G., Ayache, N., Pennec, X., 2016. A Framework for Creating Population Specific Multimodal Brain Atlas Using Clinical T1 and Diffusion Tensor Images. In: Fuster, A., Ghosh, A., Kaden, E., Rathi, Y., Reisert, M. (Eds.), Computational Diffusion MRI. Mathematics and Visualization. Springer, Cham. https://doi.org/10.1007/978-3-319-28588-7_9.

Holmes, C.J., Hoge, R., Collins, L., Woods, R., Toga, A.W., Evans, A.C., 1998. Enhancement of MR images using registration for signal averaging. J. Comput. Assist Tomogr. 22 (2), 324–333. https://doi.org/10.1097/00004728-199803000-00032.

Hsu, Y.C., Lo, Y.C., Chen, Y.J., Wedeen, V.J., Isaac Tseng, W.Y., 2015. NTU-DSI-122: a diffusion spectrum imaging template with high anatomical matching to the ICBM-152 space. Hum. Brain Mapp 36 (9), 3528–3541. https://doi.org/10.1002/hbm.22860.

Irfanoglu, M.O., Nayak, A., Jenkins, J., Hutchinson, E.B., Sadeghi, N., Thomas, C.P., Pierpaoli, C., 2016. DR-TAMAS: diffeomorphic registration for tensor accurate alignment of anatomical structures. Neuroimage 132, 439–454. https://doi.org/10.1016/j.neuroimage.2016.02.066.

Irfanoglu, M.O., Nayak, A., Jenkins, J., Pierpaoli, C., 2017. TORTOISE v3: improvements and new features of the NIH diffusion MRI processing pipeline. In: Proceedings of the 25th Annual Meeting of ISMRM Presented at the International Society for Magnetic Resonance in Medicine.

Isensee, F., Schell, M., Pflueger, I., Brugnara, G., Bonekamp, D., Neuberger, U., Wick, A., Schlemmer, H.P., Heiland, S., Wick, W., Bendszus, M., Maier-Hein, K.H., Kickingereder, P., 2019. Automated brain extraction of multisequence MRI using artificial neural networks. Hum. Brain Mapp. 40 (17), 4952–4964. https://doi.org/10.1002/hbm.24750.

Jia, Y., He, Z., Gholipour, A., Warfield, S.K., 2016. Single Anisotropic 3-D MR image upsampling via overcomplete dictionary trained from in-plane high resolution slices. IEEE J. Biomed. Health Inform 20 (6), 1552–1561. https://doi.org/10.1109/JBHI.2015.2470682.

Jones, D.K., Griffin, L.D., Alexander, D.C., Catani, M., Horsfield, M.A., Howard, R., Williams, S.C., 2002. Spatial normalization and averaging of diffusion tensor MRI data sets. Neuroimage 17 (2), 592–617.

Joshi, S., Davis, B., Jomier, M., Gerig, G., 2004. Unbiased diffeomorphic atlas construction for computational anatomy. Neuroimage 23 (1), S151–S160. https://doi.org/10.1016/j.neuroimage.2004.07.068. *Suppl.*

Kim, S.G., Jung, W.H., Kim, S.N., Jang, J.H., Kwon, J.S., 2015. Alterations of Gray and White Matter Networks in Patients with Obsessive-Compulsive Disorder: a Multimodal Fusion Analysis of Structural MRI and DTI Using mCCA+jICA. PLoS ONE 10 (6), e0127118. https://doi.org/10.1371/journal.pone.0127118.

Klein, A., Andersson, J., Ardekani, B.A., Ashburner, J., Avants, B., Chiang, M.C., Christensen, G.E., Collins, D.L., Gee, J., Hellier, P., Song, J.H., Jenkinson, M., Lepage, C., Rueckert, D., Thompson, P., Vercauteren, T., Woods, R.P., Mann, J.J., Parsey, R.V., 2009. Evaluation of 14 nonlinear deformation algorithms applied to

human brain MRI registration. Neuroimage 46 (3), 786–802. https://doi.org/10.1016/j.neuroimage.2008.12.037.
Kochunov, P., Thompson, P.M., Lancaster, J.L., Bartzokis, G., Smith, S., Coyle, T., Royall, D.R., Laird, A., Fox, P.T., 2007. Relationship between white matter fractional anisotropy and other indices of cerebral health in normal aging: tract-based spatial statistics study of aging. Neuroimage 35 (2), 478–487.
Lange, F.J., Smith, S.M., Bertelsen, M.F., Khrapichev, A.A., Manger, P.R., Mars, R.B., Andersson, J.L.R., 2020. Multimodal MRI template creation in the ring-tailed lemur and rhesus macaque. In: Špiclin, Ž., McClelland, J., Kybic, J., Goksel, O. (Eds.), Biomedical Image Registration. WBIR 2020. Lecture Notes in Computer Science, 12120. Springer, Cham. https://doi.org/10.1007/978-3-030-50120-4_14.
Lemaître, H., Crivello, F., Grassiot, B., Alpérovitch, A., Tzourio, C., Mazoyer, B., 2005. Age- and sex-related effects on the neuroanatomy of healthy elderly. Neuroimage 26 (3), 900–911. https://doi.org/10.1016/j.neuroimage.2005.02.042.
Leow, A.D., Yanovsky, I., Chiang, M.C., Lee, A.D., Klunder, A.D., Lu, A., Becker, J.T., Davis, S.W., Toga, A.W., Thompson, P.M., 2007. Statistical properties of Jacobian maps and the realization of unbiased large-deformation nonlinear image registration. IEEE Trans. Med. Imaging 26 (6), 822–832. https://doi.org/10.1109/TMI.2007.892646.
Li, Y., Verma, R., 2011. Multichannel image registration by feature-based information fusion. IEEE Trans. Med. Imaging 30 (3), 707–720. https://doi.org/10.1109/TMI.2010.2093908.
Manjón, J.V., Bertó, A., Romero, J.E., Lanuza, E., Vivo-Hernando, R., Aparici-Robles, F., Coupe, P., 2020. pBrain: a novel pipeline for Parkinson related brain structure segmentation. Neuroimage Clin 25, 102184. https://doi.org/10.1016/j.nicl.2020.102184.
Marquez, D.X., Glover, C.M., Lamar, M., Leurgans, S.E., Shah, R.C., Barnes, L.L., Aggarwal, N.T., Buchman, A.S., Bennett, D.A., 2020. Representation of older latinxs in cohort studies at the Rush Alzheimer's Disease Center. Neuroepidemiology 54 (5), 404–418. https://doi.org/10.1159/000509626.
Mazziotta, J., Toga, A., Evans, A., Fox, P., Lancaster, J., Zilles, K., Woods, R., Paus, T., Simpson, G., Pike, B., Holmes, C., Collins, L., Thompson, P., MacDonald, D., Iacoboni, M., Schormann, T., Amunts, K., Palomero-Gallagher, N., Geyer, S., Parsons, L., Mazoyer, B., 2001. A probabilistic atlas and reference system for the human brain: international Consortium for Brain Mapping (ICBM). Philos. Trans. R. Soc. Lond., B, Biol. Sci. 356 (1412), 1293–1322. https://doi.org/10.1098/rstb.2001.0915.
McCarthy, C.S., Ramprashad, A., Thompson, C., Botti, J.A., Coman, I.L., Kates, W.R., 2015. A comparison of FreeSurfer-generated data with and without manual intervention. Front. Neurosci 9, 379. https://doi.org/10.3389/fnins.2015.00379.
Mori, S., Oishi, K., Jiang, H., Jiang, L., Li, X., Akhter, K., Hua, K., Faria, A.V., Mahmood, A., Woods, R., Toga, A.W., Pike, G.B., Neto, P.R., Evans, A., Zhang, J., Huang, H., Miller, M.I., van Zijl, P., Mazziotta, J., 2008. Stereotaxic white matter atlas based on diffusion tensor imaging in an ICBM template. Neuroimage 40 (2), 570–582. https://doi.org/10.1016/j.neuroimage.2007.12.035.
Niaz, M.R., Wu, Y., Ridwan, A.R., Qi, X., Zhang, S., Bennett, D.A., Arfanakis, K., 2020. Development and evaluation of a high spatial resolution diffusion tensor template of the older adult human brain. In: Proceedings of the 28th Annual Meeting of ISMRM Presented at the International Society for Magnetic Resonance in Medicine.
Niaz, M.R., Ridwan, A.R., Wu, Y., , Alzheimer's Disease Neuroimaging Initiative, Bennett, D.A., Arfanakis, K., 2022. Development and evaluation of a high resolution 0.5mm isotropic T1-weighted template of the older adult brain. Neuroimage 248, 118869. https://doi.org/10.1016/j.neuroimage.2021.118869.
Nyúl, L.G., Udupa, J.K., Zhang, X., 2000. New variants of a method of MRI scale standardization. IEEE Trans. Med. Imaging 19 (2), 143–150. https://doi.org/10.1109/42.836373.
Park, H.J., Kubicki, M., Shenton, M.E., Guimond, A., McCarley, R.W., Maier, S.E., Kikinis, R., Jolesz, F.A., Westin, C.F., 2003. Spatial normalization of diffusion tensor MRI using multiple channels. Neuroimage 20 (4), 1995–2009. https://doi.org/10.1016/j.neuroimage.2003.08.008.
Park, M.T., Pipitone, J., Baer, L.H., Winterburn, J.L., Shah, Y., Chavez, S., Schira, M.M., Lobaugh, N.J., Lerch, J.P., Voineskos, A.N., Chakravarty, M.M., 2014. Derivation of high-resolution MRI atlases of the human cerebellum at 3T and segmentation using multiple automatically generated templates. Neuroimage 95, 217–231. https://doi.org/10.1016/j.neuroimage.2014.03.037.
Pierpaoli, C., Walker, L., Irfanoglu, M.O., Barnett, A., Basser, P., Chang, L.C., Koay, C., Pajevic, S., Rohde, G., Sarlls, J., Wu, M., 2010. TORTOISE: an integrated software package for processing of diffusion MRI data. In: Proceedings of the 18th Annual Meeting of ISMRM Presented at the International Society for Magnetic Resonance in Medicine.
Radua, J., Canales-Rodríguez, E.J., Pomarol-Clotet, E., Salvador, R., 2014. Validity of modulation and optimal settings for advanced voxel-based morphometry. Neuroimage 86, 81–90. https://doi.org/10.1016/j.neuroimage.2013.07.084.
Raz, N., Lindenberger, U., Rodrigue, K.M., Kennedy, K.M., Head, D., Williamson, A., Dahle, C., Gerstorf, D., Acker, J.D., 2005. Regional brain changes in aging healthy adults: general trends, individual differences and modifiers. Cerebral Cortex 15 (11), 1676–1689.
Reinhold, J.C., Dewey, B.E., Carass, A., Prince, J.L., 2019. Evaluating the impact of intensity normalization on MR Image Synthesis. In: Proceedings of SPIE–the International Society for Optical Engineering, 10949, 109493H. https://doi.org/10.1117/12.2513089.
Ridwan, A.R., Niaz, M.R., Wu, Y., Qi, X., Zhang, S., Kontzialis, M., Javierre-Petit, C., Tazwar, M., , Alzheimer's Disease Neuroimaging Initiative, Bennett, D.A., Yang, Y., Arfanakis, K., 2021a. Development and evaluation of a high performance T1-weighted brain template for use in studies on older adults. Hum Brain Mapp 42 (6), 1758–1776. https://doi.org/10.1002/hbm.25327.
Ridwan, A.R., Wu, Y., Niaz, M.R., Bennett, D.A., Arfanakis, K., 2021b. Construction of an unbiased high resolution and detail-preserving structural T1-weighted template for use in studies on older adults. In: Proceedings of the 29th Annual Meeting of ISMRM Presented at the International Society for Magnetic Resonance in Medicine.
Rohde, G.K., Barnett, A.S., Basser, P.J., Marenco, S., Pierpaoli, C., 2004. Comprehensive approach for correction of motion and distortion in diffusion-weighted MRI. Magn Reson Med 51 (1), 103–114. https://doi.org/10.1002/mrm.10677.
Rohlfing, T., Kroenke, C.D., Sullivan, E.V., Dubach, M.F., Bowden, D.M., Grant, K.A., Pfefferbaum, A., 2012. The INIA19 template and NeuroMaps atlas for primate brain image parcellation and spatial normalization. Front Neuroinform 6, 27. https://doi.org/10.3389/fninf.2012.00027.
Rohlfing, T., Zahr, N.M., Sullivan, E.V., Pfefferbaum, A., 2010. The SRI24 multichannel atlas of normal adult human brain structure. Hum Brain Mapp 31 (5), 798–819.
Sasamoto, A., Miyata, J., Kubota, M., Hirao, K., Kawada, R., Fujimoto, S., Tanaka, Y., Hazama, M., Sugihara, G., Sawamoto, N., Fukuyama, H., Takahashi, H., Murai, T., 2014. Global association between cortical thinning and white matter integrity reduction in schizophrenia. Schizophr Bull 40 (2), 420–427.
Schwarz, C.G., Gunter, J.L., Ward, C.P., Vemuri, P., Senjem, M.L., Wiste, H.J., Petersen, R.C., Knopman, D.S., Jack, C.R., 2017. The Mayo Clinic adult lifespan template: better quantification across the lifespan. Alzheimer's Dement 13, P792.
Seghers, D., D'Agostino, E., Maes, F., Vandermeulen, D., Suetens, P, 2004. Construction of a brain template from MR images using state-of-the-art registration and segmentation techniques. In: Medical Image Computing and Computer-Assisted Intervention–MICCAI 2004: 7th International Conference, Saint-Malo, France, September 26-29, 2004. Springer Berlin Heidelberg, pp. 696–703. Proceedings, Part I 7.
Senjem, M.L., Gunter, J.L., Shiung, M.M., Petersen, R.C., Jack Jr, C.R., 2005. Comparison of different methodological implementations of voxel-based morphometry in neurodegenerative disease. Neuroimage 26 (2), 600–608.
Shah, M., Xiao, Y., Subbanna, N., Francis, S., Arnold, D.L., Collins, D.L., Arbel, T., 2011. Evaluating intensity normalization on MRIs of human brain with multiple sclerosis. Med Image Anal 15 (2), 267–282. https://doi.org/10.1016/j.media.2010.12.003.
Shi, F., Wang, L., Wu, G., Li, G., Gilmore, J.H., Lin, W., Shen, D., 2014. Neonatal atlas construction using sparse representation. Hum Brain Mapp 35 (9), 4663–4677. https://doi.org/10.1002/hbm.22502.
Sullivan, E.V., Adalsteinsson, E., Pfefferbaum, A., 2006. Selective age-related degradation of anterior callosal fiber bundles quantified in vivo with fiber tracking. Cerebral Cortex 16 (7), 1030–1039.
Sullivan, E.V., Rohlfing, T., Pfefferbaum, A., 2010. Quantitative fiber tracking of lateral and interhemispheric white matter systems in normal aging: relations to timed performance. Neurobiol. Aging 31 (3), 464–481.
Sydykova, D., Stahl, R., Dietrich, O., Ewers, M., Reiser, M.F., Schoenberg, S.O., Möller, H. J., Hampel, H., Teipel, S.J., 2007. Fiber connections between the cerebral cortex and the corpus callosum in Alzheimer's disease: a diffusion tensor imaging and voxel-based morphometry study. Cerebral cortex 17 (10), 2276–2282. https://doi.org/10.1093/cercor/bhl136. New York, N.Y.: 1991.
Sánchez, I., & Vilaplana, V. (2018). Brain MRI super-resolution using 3D generative adversarial networks. *arXiv preprint* arXiv:1812.11440.
Toga, A.W., Thompson, P.M., Mori, S., Amunts, K., Zilles, K., 2006. Towards multimodal atlases of the human brain. Nat. Rev. Neurosci. 7 (12), 952–966.
Tustison, N.J., Avants, B.B., Cook, P.A., Zheng, Y., Egan, A., Yushkevich, P.A., Gee, J.C., 2010. N4ITK: improved N3 bias correction. IEEE Trans Med Imaging 29 (6), 1310–1320. https://doi.org/10.1109/TMI.2010.2046908.
Van Leemput, K., Bakkour, A., Benner, T., Wiggins, G., Wald, L.L., Augustinack, J., Dickerson, B.C., Golland, P., Fischl, B., 2008. Model-based segmentation of hippocampal subfields in ultra-high resolution in vivo MRI. MICCAI ... Int. Conference Med. Image Comput. Comp.-Assisted Interv 11 (Pt 1), 235–243. https://doi.org/10.1007/978-3-540-85988-8_29.
Wang, Y., Xu, M., Geng, L., Zhao, Y., Guo, Z., Fan, Y., Niu, Y., 2022. DTI Atlases Evaluations. Neuroinformatics 20 (2), 327–351. https://doi.org/10.1007/s12021-021-09521-y.
Wang, Z., Bovik, A.C., Sheikh, H.R., Simoncelli, E.P., 2004. Image quality assessment: from error visibility to structural similarity. IEEE Transac. Image Process 13 (4), 600–612.
Westlye, L.T., Walhovd, K.B., Dale, A.M., Bjørnerud, A., Due-Tønnessen, P., Engvig, A., Grydeland, H., Tamnes, C.K., Ostby, Y., Fjell, A.M., 2010. Life-span changes of the human brain white matter: diffusion tensor imaging (DTI) and volumetry. Cerebral Cortex 20 (9), 2055–2068.
Wicks, P., Vaughan, T.E., Massagli, M.P., Heywood, J., 2011. Accelerated clinical discovery using self-reported patient data collected online and a patient-matching algorithm. Nat. Biotechnol. 29 (5), 411–414. https://doi.org/10.1038/nbt.1837.
Wiggins, G.C., Triantafyllou, C., Potthast, A., Reykowski, A., Nittka, M., Wald, L.L., 2006. 32-channel 3 Tesla receive-only phased-array head coil with soccer-ball element geometry. Magn. Reson. Med 56 (1), 216–223. https://doi.org/10.1002/mrm.20925.
Wu, Y., Ridwan, A.R., Niaz, M.R., Qi, X., Zhang, S., , Alzheimer's Disease Neuroimaging Initiative, Bennett, D.A., Arfanakis, K., 2022. Development of high quality T1-weighted and diffusion tensor templates of the older adult brain in a common space. Neuroimage 260, 119417. https://doi.org/10.1016/j.neuroimage.2022.119417.
Yanovsky, I., Leow, A.D., Lee, S., Osher, S.J., Thompson, P.M., 2009. Comparing registration methods for mapping brain change using tensor-based morphometry. Med Image Anal 13 (5), 679–700. https://doi.org/10.1016/j.media.2009.06.002.
Yoon, U., Fonov, V.S., Perusse, D., Evans, A.C., Brain Development Cooperative Group, 2009. The effect of template choice on morphometric analysis of pediatric brain data. Neuroimage 45 (3), 769–777.

Yushkevich, P.A., Avants, B.B., Pluta, J., Das, S., Minkoff, D., Mechanic-Hamilton, D., Glynn, S., Pickup, S., Liu, W., Gee, J.C., Grossman, M., Detre, J.A., 2009. A high-resolution computational atlas of the human hippocampus from postmortem magnetic resonance imaging at 9.4 T. Neuroimage 44 (2), 385–398. https://doi.org/10.1016/j.neuroimage.2008.08.042.

Yushkevich, P.A., Pluta, J.B., Wang, H., Xie, L., Ding, S.L., Gertje, E.C., Mancuso, L., Kliot, D., Das, S.R., Wolk, D.A., 2015. Automated volumetry and regional thickness analysis of hippocampal subfields and medial temporal cortical structures in mild cognitive impairment. Hum Brain Mapp 36 (1), 258–287. https://doi.org/10.1002/hbm.22627.

Zeng, K., Zheng, H., Cai, C., Yang, Y., Zhang, K., Chen, Z., 2018. Simultaneous single- and multi-contrast super-resolution for brain MRI images based on a convolutional neural network. Comput. Biol. Med. 99, 133–141. https://doi.org/10.1016/j.compbiomed.2018.06.010.

Zhang, H., Yushkevich, P.A., Rueckert, D., Gee, J.C., 2010. A Computational White Matter Atlas for Aging with Surface-Based Representation of Fasciculi. In: Fischer, B., Dawant, B.M., Lorenz, C. (Eds.), Biomedical Image Registration. WBIR 2010. Lecture Notes in Computer Science, Vol 6204. Springer, Berlin, Heidelberg. https://doi.org/10.1007/978-3-642-14366-3_8.

Zhang, S., Arfanakis, K., 2018. Evaluation of standardized and study-specific diffusion tensor imaging templates of the adult human brain: template characteristics, spatial normalization accuracy, and detection of small inter-group FA differences. Neuroimage 172, 40–50. https://doi.org/10.1016/j.neuroimage.2018.01.046.

Zhang, S., Peng, H., Dawe, R.J., Arfanakis, K., 2011. Enhanced ICBM diffusion tensor template of the human brain. Neuroimage 54 (2), 974–984. https://doi.org/10.1016/j.neuroimage.2010.09.008.

Zhang, Z.G., Chan, S.C., Zhang, X., Lam, E.Y., Wu, E.X., Hu, Y., 2009. High-resolution reconstruction of human brain MRI image based on local polynomial regression. In: Proceedings of the 4th International IEEE/EMBS Conference on Neural Engineering, pp. 245–248. https://doi.org/10.1109/NER.2009.5109279. NER '09.

Zhao, C., Carass, A., Jog, A., Prince, J.L., 2016. Effects of Spatial Resolution on Image Registration. In: Proceedings of SPIE–the International Society for Optical Engineering, 9784, p. 97840Y. https://doi.org/10.1117/12.2217322.